Miocene uplift of the NE Greenland margin linked to plate tectonics: Seismic evidence from the Greenland Fracture Zone, NE Atlantic

Margin Uplift and Plate Tectonics

Døssing Andreasen, Arne; Japsen, Peter; Watts, Anthony B.; Nielsen, Tove; Jokat, Wilfried; Thybo, Hans; Dahl-Jensen, Trine

Published in:
Tectonics

Link to article, DOI:
10.1002/2015tc004079

Publication date:
2016

Document Version
Peer reviewed version

Miocene uplift of the NE Greenland margin linked to plate tectonics: Seismic evidence from the Greenland Fracture Zone, NE Atlantic.

Arne Døssing[1,*], Peter Japsen[2], Anthony B. Watts[3], Tove Nielsen[2], Wilfried Jokat[4,5], Hans Thybo[6], Trine Dahl-Jensen[2]

1. DTU Space, Technical University Denmark, Diplomvej 371, 2800 Lyngby, Denmark
2. Geological Survey of Denmark and Greenland (GEUS), Øster Voldgade 10, 1350 Copenhagen, Denmark
3. Department of Earth Sciences, University of Oxford, UK.
4. Alfred Wegener Institute Helmholtz Centre for Polar and Marine Research, Am Handelshafen 12, D-27570 Bremerhaven, Germany
5. Geoscience Department, University of Bremen, D-28359 Bremen, Germany
6. Department of Geosciences and Natural Resource Management, University of Copenhagen, Øster Voldgade 10, 1350 Copenhagen, Denmark

* Corresponding author

This article has been accepted for publication and undergone full peer review but has not been through the copyediting, typesetting, pagination and proofreading process which may lead to differences between this version and the Version of Record. Please cite this article as doi: 10.1002/2015TC004079

ABSTRACT

Tectonic models predict that, following breakup, rift margins undergo only decaying thermal subsidence during their post-rift evolution. However, post-breakup stratigraphy beneath the NE Atlantic shelves shows evidence of regional-scale unconformities, commonly cited as outer margin responses to inner margin episodic uplift, including the formation of coastal mountains. The origin of these events remains enigmatic. We present a seismic reflection study from the Greenland Fracture Zone – East Greenland Ridge (GFZ-EGR) and the NE Greenland shelf. We document a regional intra-Miocene seismic unconformity (IMU), which marks the termination of syn-rift deposition in the deep-sea basins and onset of: (i) thermo-mechanical coupling across the GFZ, (ii) basin compression, and (iii) contourite deposition, north of the EGR. The onset of coupling across the GFZ is constrained by results of 2-D flexural backstripping. We explain the thermo-mechanical coupling and the deposition of contourites by the formation of a continuous plate boundary along the Mohns and Knipovich ridges, leading to an accelerated widening of the Fram Strait. We demonstrate that the IMU event is linked to onset of uplift and massive shelf-progradation on the NE Greenland margin. Given an estimated middle-to-late Miocene (~15-10 Ma) age of the IMU, we speculate that the event is synchronous with uplift of the East and West Greenland margins. The correlation between margin uplift and plate-motion changes further indicates that the uplift was triggered by plate tectonic forces, induced perhaps by a change in the Iceland plume (a hot pulse) and/or by changes in intra-plate stresses related to global tectonics.

1. Introduction

Regional seismic reflection studies from the North-East (NE) Greenland shelf (Figure 1) (Hamann et al. 2005; Berger and Jokat, 2008; 2009) document several, up to 200 km wide progradational wedges, which are bounded below by a distinct angular unconformity (Figure 2). The clastic wedges constitute large parts of the present-day NE Greenland shelf as well as the eastern Greenland shelves further south (Larsen and Saunders, 1998; Berger and Jokat, 2008; 2009). Their formation is attributed to early or mid/late-Miocene and later episodic uplift events of the inner margin, combined with glacial erosion and successive advances of the Greenland ice-sheet onto the shelf (Larsen et al., 1994; Hamann et al., 2005; Berger and Jokat, 2008; 2009). Likewise, the Cenozoic sedimentary basins beneath other continental shelves of the NE Atlantic contain a remarkable record of regional unconformities, suggested to reflect episodic Neogene inner margin uplift events (e.g., Eidvin et al., 2000; Løseth and Henriksen, 2005; Rundberg and Eidvin, 2005; Japsen et al., 2007; Holford et al., 2009; Stoker et al., 2005; 2010; Eidvin et al., 2014 and refs. therein) and/or phases of mild compression (Lundin and Doré, 2002; Doré et al., 2008).

High coastal mountains, which fringe the shelves in eastern Greenland, mid-southern Norway and the western British Isles, are commonly inferred to be products of the Neogene episodic uplift (Hansen et al., 1996; Thomson et al., 1999; Johnson and Gallagher, 2000; Japsen et al., 2012a; Holford et al., 2009; Bonow et al., 2014). This is particularly well documented in East Greenland (68 – 71°N), where thick (>7 km) breakup-related flood basalts are found at elevations up to 3.7 km above sea level (Brooks, 2011). Geological evidence (Larsen and Tegner, 2006; Bonow et al., 2014) documents a landscape that was low-lying during breakup and subsequently affected by km-scale uplift events (Hansen, 1996; Larsen and Saunders, 1998; Brooks, 2011; Bonow et al., 2014; Japsen et al., 2014).

The Neogene uplift events are a matter of wide debate (Anell et al., 2009). In short, they are often inferred to relate to, e.g., plate-motion compressional stresses (Cloetingh et al., 1990; Holford et al., 2009; Stoker et al., 2010; Japsen et al., 2012a;b), dynamic uplift (Rohrman and van der Beek, 1996; Arrowsmith et al., 2005; Rickers et al., 2013; Japsen et al., 2014; Steinberger et al., 2015), and/or climate changes towards lower temperatures, with increased alpine glaciation and erosion acting as a true global exhumation agent together with buoyant isostatic forces (Molnar and England, 1990; Nielsen et al., 2009; Pedersen et al., 2012; Steinberger et al., 2015). A key problem for the climate argumentation is, e.g., that much of Greenland's topography was probably not caused by ice-related processes (Japsen et al., 2006; Medvedev et al., 2013). On the other hand, a key problem for the non-climate

argumentation is the uncertainty of pin pointing the single tectonic uplift force and the precise correlation to known plate tectonic events.

In this study, we present a seismic tectono-stratigraphic analysis of sedimentary layers deposited against the Greenland Fracture Zone (GFZ), located off the NE Greenland shelf (Figure 1). The GFZ has played a key role in the opening of the northern NE Atlantic and has undergone a complex tectonic evolution due to multiple changes in relative spreading directions during the Cenozoic (Mosar et al., 2002; Døssing et al., 2008; Døssing and Funck, 2012). Such changes in the lithospheric stress field affect transform fault systems by imposing components of compression and/or extension across the transform, thereby affecting its thermo-mechanical properties and, hence, tectonic subsidence across it (Wessel and Haxby, 1990; Lorenzo and Wessel, 1997). Seismic stratigraphic analysis of sedimentary layers deposited against the GFZ may, therefore, be used to infer its thermo-mechanical history (Mascle and Blarez, 1987; Lorenzo and Wessel, 1997; Clift et al., 1997) and important plate kinematic events. By using published and previously unpublished seismic reflection data, we are able to correlate the stratigraphy against the GFZ with the post-breakup stratigraphy beneath the NE Greenland shelf. We make use of the tectonic subsidence history across the GFZ to explain the onset of the Miocene uplift and shelf progradation in NE Greenland. All ages in this study are according to the Gradstein et al. (2012) time scale.

2. Geological setting

2.1. Tectono-bathymetric features

The GFZ is located in the northern NE Atlantic and strikes roughly perpendicular to the NE Greenland shelf (Figures 1, 3). Here, the fracture zone constitutes the steep southern flank of the East Greenland Ridge (EGR), which juts out from the widest part of the NE Greenland shelf and continues for ~300 km to the south-east as an elongated, 30-km-wide bathymetric high (Døssing et al., 2008; Døssing and Funck, 2012). The GFZ defines a sharp boundary between the EGR and the flat Greenland Basin floor, which is delimited toward the south and east by the Jan Mayen Fracture Zone and the Mohns Ridge, respectively (Figures 1, 3). At its easternmost end, the GFZ-EGR turns into an east-west direction and gradually merges with the rugged flank of the Mohns-Knipovich Ridge system.

The flat seafloor of the Boreas Basin is located to the north of the EGR and is bounded to the west, east and north by the NE Greenland shelf, the Knipovich Ridge and the Hovgaard

Ridge, respectively (Figure 3). In its southwestern most part, the Boreas Basin juxtaposes the deep, elongated Greenland Fracture Zone Basin Province (GFZBP), which is delimited to the southwest by a branch of the GFZ that separates the GFZBP from the NE Greenland shelf (Døssing and Funck, 2012).

2.2. Regional tectonic development

Continental breakup and seafloor spreading of the NE Atlantic commenced at the Paleocene-Eocene transition (chron C24B) along three inter-connected spreading ridges: Reykjanes Ridge, Aegir Ridge and Mohns Ridge (Talwani and Eldholm, 1977; Hagevang et al., 1983). In the northern NE Atlantic, the Paleogene extensional stresses were accommodated by a major left-stepping, ridge-transform-ridge system (Figure 4a) that consisted of the Mohns Ridge, the GFZ and a zone of continental shear rifting – or seafloor spreading – in the western Boreas Basin (Mosar et al., 2002; Engen et al., 2008; Døssing and Funck, 2012). During an early to late Oligocene (chron C13 – C7) regional plate reorganization (Srivastava and Tapscott, 1986; Mosar et al., 2002), the rift axis in the western Boreas Basin shifted eastward to proto-Knipovich Ridge segments (Figure 4b) and promoted a northwards propagation of the Mohns Ridge. This led to severe extension across the GFZ as well as transform fault migration and ultimately the separation of the continental EGR from the Barents Sea paleo-margin (Døssing et al., 2008; Engen et al., 2008; Faleide et al., 2008; Døssing and Funck, 2012). These plate motion changes may also have facilitated the onset of seafloor spreading in the Boreas Basin at chron C9 time (Ehlers and Jokat, 2009; Hermann and Jokat, 2013). Today, the GFZ separates magnetic chrons C24B-C7 oceanic crust of the Greenland Basin from highly extended continental crust of the EGR (and the GFZBP) (Døssing et al., 2008; Døssing and Funck, 2012) and crust of probably oceanic origin and/or exhumed upper mantle beneath the Boreas Basin (Figure 4c) (Hermann and Jokat, 2013; Gerlings et al., 2014). As such, the EGR-GFZBP defines a continental transform margin against the GFZ (Døssing and Funck, 2012).

At some time between the late early Miocene (chron C6 time) and late Miocene (chron C5 time), the Mohns and Knipovich ridges eventually merged to form a continuous plate boundary. At the same time, onset of the present-day mode of seafloor spreading was established along all spreading segments to the north of the GFZ (Vogt, 1986; Mosar et al., 2002; Doré et al., 2008; Engen et al., 2008).

3. Data sets

Due to the pack-ice and icebergs, the NE Greenland shelf remains largely underexplored in terms of traditional marine geophysical surveys. Moreover, no deep wells have so far been drilled on the eastern shelves of Greenland. Hinz et al. (1987) provided the first insight into the sedimentary and tectonic evolution of the NE Greenland shelf, based on a seismic reflection profile recorded in 1981. Another seismic survey (KANUMAS), carried out from 1991 to 1995, gathered conventional 2-D Multi-channel seismic (MCS) data in a very open grid in the area between 72°N and 79°N (Figure 3). To advance in the understanding in the tectonic and glacial history of the outer NE Greenland margin, 2-D MCS data were subsequently collected by the Alfred Wegener Institute for Polar and Marine Research (AWI). Data were collected north of the GFZ in 2002 (Jokat et al., 2003; Berger and Jokat, 2009) and south of the GFZ in 2003 (Jokat et al., 2004; Berger and Jokat, 2008). The resulting seismic surveys, AWI-2002 and AWI-2003, cover the entire outer shelf and slope between 71°30´N and 80°30´N, as well as the northwestern part of the GFZ-EGR, the western part of the Boreas Basin and part of the Molloy Basin (Figure 3). In 2002, three additional, high quality 2-D MCS profiles were also acquired in the deep-sea – along, across and south of – the GFZ-EGR by the Geological Survey of Denmark and Greenland (GEUS) during the GEUS2002NEG marine geophysical survey (Døssing et al., 2008). Acquisition and processing details for the KANUMAS, AWI2002, AWI2003 and GEUS2002NEG seismic surveys, respectively, are described in Hamann et al. (2005), Berger and Jokat (2008; 2009), and Døssing et al. (2008).

In this study, we present four seismic profiles compiled from the above surveys. The profiles are highlighted in Figure 3. Profile 1 is 420-km-long and transects the entire NE Greenland shelf as well as C24 oceanic crust of the Greenland Basin. The inner part of this profile is here presented as a seismic geo-section, originally compiled by Hamann et al. (2005), while the outer part is composed of line AWI2003-0390 of the AWI2003 survey. A seismic interpretation of this line was published by Berger and Jokat (2008). The 100-km-long Profile 2 is parallel to – and located north of – Profile 1, where it transects the outer shelf slope as well as magnetic chrons C24B – C23 oceanic crust of the Greenland Basin. Profile 2 is composed by line GEUS2002NEG-3 which has not been published before. Profile 3 is 270-km-long and strikes almost perpendicular to Profile 2. The two profiles intersect in the Greenland Basin about 20 km to the south of the GFZ. Profile 3 transects the GFZ-EGR at high angle as well as magnetic chrons C22 – C23 oceanic crust of the Greenland Basin and continental crust of the GFZBP. The profile is composed of parts of lines AWI2003-0165 and

GEUS2002NEG-1. While GEUS2002NEG-1 has been published with a simple line drawing of sedimentary structures together with deep-seismic data (Døssing et al., 2008), line AWI2003-0165 has not been published before. The final Profile 4 is only 90 km long and transects the GFZ-EGR-GFZBP at high angle, about 40 km east of Profile 3 (Figure 3). Profile 4 constitutes the northern part of line GEUS2002NEG-1.

We supplement the seismic Profiles 1 – 4 with an additional, composite seismic profile shown in Supplementary Material (Figures S1, S2). We also make use of a map of calculated 1st vertical derivatives of the magnetic anomaly field (Figure 5).

4. POST-BREAKUP STRATIGRAPHY BENEATH THE NE GREENLAND SHELF

The post-breakup, Cenozoic sedimentary successions beneath the NE Greenland shelf have been mapped and described by Hamann et al. (2005) and Berger and Jokat (2008; 2009). Here, we summarize the Cenozoic stratigraphic evolution of the shelf before proceeding to the seismic results of Døssing et al. (this study) from the adjacent GFZ area. We highlight the Cenozoic stratigraphy of the NE Greenland shelf in Profile 1 (Figures 3, 6).

Hamann et al. (2005) subdivide the NE Greenland shelf into roughly northeast oriented, major tectonic elements, based on seismic interpretation of KANUMAS data. South of 75°N, the shelf basins are dominated by Cenozoic plateau basalts, which obscure the seismic signal from the deeper succession. North of here, seismic data indicate an up to 8 s TWT thick and fairly complete succession of inferred Devonian to Neogene age (Figure 6). In the younger sedimentary section, Hamann et al. (2005) trace a pronounced, north-south trending erosional unconformity (Figure 6; red line). This unconformity was first reported by Hinz et al. (1993). Progressively older, aggrading seismic units are tilted and truncated landwards below the unconformity (Figure 6; km 0 – 180), whereas the overlying mega-sequence shows distinct seaward progradation and apparent onlap towards the shelf (Figure 6; km 180 – 350). Hamann et al. (2005) attribute the formation of this unconformity at the base of progradation to basin margin uplift initiated during the earliest Miocene. They based their age estimation on correlation with regional stratigraphic events elsewhere in the NE Atlantic and onshore eastern Greenland. We hereafter refer to the unconformity as the *Intra Miocene Unconformity* (IMU). Hamann et al. (2005) further identify low-amplitude folds and reverse, margin-parallel faults, with throws up to 200 m, in relation to the IMU (Figure 6; km 125). They attribute these features to mild compression. In support of this, margin-parallel, open folds have been found on Traill Ø in NE Greenland (location in Figure 1) and likewise interpreted

as evidence of post-breakup compression. Although their specific age is not well constrained, it is suggested to be late Cenozoic (Price et al., 1997).

The southeastern part of Profile 1 ties with ODP-site 913 (Figures 3, 6). By correlating the IMU reflector (Supplementary Material Figures S1, S2) within the seismic network from the shelf to the ODP-site 913 (Myhre et al., 1995a), Berger and Jokat (2008) could confirm the proposed Miocene age of the IMU on the shelf within drilling results. Berger and Jokat (2009) further show that the IMU can be traced as far south as the East Greenland shelf near 68°N (Figure 2c). South of here, however, the overlying prograding wedge appears to be younger (Berger and Jokat, 2009). In accordance with Hamann et al. (2005), Berger and Jokat (2008; 2009) attribute the formation of the IMU to relative inner margin uplift, combined with glacial erosion and successive advances of the Greenland ice-sheet onto the shelf.

The stratigraphic correlation of Berger and Jokat (2008) to ODP-site 913 shows that the seismic mega units immediately below and above the IMU (here referred to as Unit I and Unit II, respectively) correspond to the transition between Unit II (silty clay and clay) and Unit III (coarser beds of clayey, silty, and sandy muds) of Myhre et al. (1995a). However, ODP-site 913 had very poor recovery (~2%) around the IMU interval, and the transition between their Units II and III is within a wash core. Thus, it is placed at the lowest occurrence of beds of clayey, silty, and sandy muds at 378.7 mbsf. (meter below seafloor) in Core 151-913B-19W. This interpretation is supported by moderately, well-preserved Miocene diatoms, radiolarians and benthic foraminifers recovered at slightly deeper levels at 423.5 mbsf. Myhre et al., (1995a) suggest a middle-to-late Miocene age for the overlying washed section. They further suggest that the age of their Unit II to Unit III transition (i.e. the IMU) is within the middle Miocene (~15 Ma), and that it represents a change from predominantly non-glacial deposition in their Unit II to glacial deposition in their Unit III. This interpretation is based on a similarity in composition and texture of sediments in their Unit III with Pliocene glacial sediments higher in the stratigraphy. Lack of abundant dropstones in their Unit III, however, compared with the distinctive Pliocene glacial units is suggested to reflect only little ice-rafting activity during the late Miocene to Pliocene.

To the north of the GFZ-EGR (Figure 3) Berger and Jokat (2009) use the AWI2002 survey to trace another, prominent seismic unconformity throughout the Boreas and Molloy basins. They further use ODP-site 909 stratigraphy (Myhre et al., 1995b) to constrain the reflector age. This site, with a high recovery rate, provided an age of earliest Miocene for the oldest sediments (Hull et al., 1996). Seismic-to-borehole tie (Berger and Jokat, 2009) shows the mapped unconformity is situated in the middle of the 400-m-thick lithological Unit IIIa of

Myhre et al. (1995b), which is composed of silty clay, clayey mud and carbonate-bearing clay. Unfortunately, the prominent reflector of the unconformity was not dated. However, according to Myhre et al. (1995b) the entire interval of Unit IIIa is Miocene in age, with Pliocene to Miocene sediments above and Miocene to upper Oligocene sediments below. In concordance with the suggested middle Miocene age (~15 Ma) of the IMU south of the GFZ-EGR, Berger and Jokat (2009), therefore, assign a middle Miocene age (~15 Ma) for the regional unconformity to the north of the GFZ-EGR. This interpretation is based on the assumption of a constant sedimentation rate for Unit IIIa of Myhre et al. (1995b). Thus, by combining the seismic results, north and south of the GFZ-EGR, Berger and Jokat (2009) suggest the IMU (Figure 6) represents a regional middle Miocene unconformity, which is traceable beneath the inner and outer eastern Greenland shelves and beneath the adjoining deep-sea basins between 72°N and 81°N.

Subsequent re-analysis of the ODP-site 913 borehole data (Hull et al., 1996; Poulsen et al., 1996) favor a late Miocene age of the IMU reflector to the south of the GFZ. Likewise, re-analysis of the ODP-site 909 borehole data (Hull et al., 1996) suggests the sediments of Unit IIIa of Myhre et al. (1995b) to be of middle to late Miocene age, that is, the depth of the IMU reflector in ODP-site 909 appears to define the transition from middle to upper Miocene sediments according to Hull et al. (1996) rather than from early to middle Miocene (Myhre et al., 1995b; Berger and Jokat, 2009).

Considering the uncertainties related to the dating of the IMU reflector in ODP-sites 909 and 913, we therefore prefer the age of this regional event, to the north and south of the GFZ, to be within the middle-to-late Miocene.

5. RESULTS

We have mapped the seismic Units I and II of Profile 1 (Figure 6) in the deep-sea sedimentary successions of the Greenland Basin and the GFZBP, using the seismic network to the south and north of the GFZ (Figure 3). Here, we present an interpretation of the stratigraphy and basin evolution across the GFZ, with particular focus on the regional IMU surface. Our seismic interpretations are highlighted in Profiles 2 – 4 (Figures 3, 7 – 9). We substantiate our seismic interpretations by a subsequent analysis of the tectonic subsidence history against the GFZ. For this, we use the results of 2-D flexure modeling and 2-D backstripping calculations of seismic layers identified in the Greenland Basin-part of Profile 3.

5.1. Greenland Basin

In Profile 2 (Figure 7), the flat seafloor of the Greenland Basin is located around 4.9 s TWT. It is underlain by a 2.0 – 2.6 s TWT thick sedimentary layer that drapes a rough basement surface. The oceanic basement (Figure 7; km 55 – 100) is dissected by numerous, closely spaced and seaward-dipping faults, whereas two, 15-km-wide grabens outline the continent-ocean transition zone (COT). The COT is characterized by highly extended continental crust (Voss et al., 2009), with a maximum basement depth of 7.4 s TWT along the profile. A prominent, seaward-dipping base-of-slope fault (BSF), with an offset of 1.8 s TWT, separates shallow basement beneath the outer NE Greenland shelf from deep basement of the COT. The BSF further controls the location of a margin-parallel bathymetric escarpment, located between the outer shelf slope and the Greenland Basin. This escarpment correlates southwards with the basement ridge observed beneath the outer shelf slope in Profile 1 (Figures 3, 6).

In Profile 3 (Figure 8), the seafloor of the Greenland Basin is underlain by a 0.5 – 2.5 s TWT thick sedimentary layer that drapes oceanic basement of early Eocene age (chron C22 – C23; cf. Figure 5). The oceanic basement exhibits a pronounced down-flexure towards the GFZ-EGR and reaches a maximum depth of 7.5 s TWT against the fracture zone (Figure 8b). The basement flexure is associated with an outer flexural basement rise about 130 km south-southwest of the GFZ, with basement depths of 5.4 s TWT. Southwards, the oceanic basement deepens again. This long wavelength, oceanic basement flexure against the GFZ is well-imaged in Bouguer anomaly data (Supplementary Material, Figure S3). Similar to Profile 2, the oceanic basement in Profile 3 (Figure 8b: km 0 – 165) is dissected by numerous normal faults, in particular in the outer rise region.

In Profile 2 (Figure 7), the thickness of Unit I generally increase from 0.5 s TWT in the southeast at magnetic chron ~C23 oceanic crust to almost 2.0 s TWT against the BSF. A similar geometry is found in Profile 2, where Unit I forms a broad, wedge-shaped accumulation that thickens from overall 0.2 s TWT in the south-southwest to ~1.2 s TWT against the GFZ-EGR (Figure 8; km 0 – 165). We identify two subunits in Unit I of the Greenland Basin: Subunit Ia and Ib from deepest to shallowest. The subunits display overall wedge-shaped geometries and contain diverging reflections toward the bounding faults. We interpret this pattern as syn-sedimentary infill of fault-controlled basins. Subunits Ia and Ib are further defined by stratified, semi-continuous reflections, indicating dominantly hemipelagic, subtle deposition. This interpretation is supported by borehole information from ODP-site 913, with findings of middle Eocene to middle Miocene, massive and laminated

clay, silty clay, mud and biosillica below the IMU (Myhre et al., 1995a; Hull et al., 1996; Berger and Jokat, 2008).

Unit II unconformably overlies the IMU (Figures 7, 8). In Profile 2, the unit thins markedly from more than 1.0 s TWT in the southeast to ~0.2 s TWT near the BSF, whereas the unit is ~0.7 – 1.0 s TWT thick along the Greenland Basin-part of Profile 3, thickest near the GFZ (Figure 8b). We distinguish between three subunits in Unit II of the Greenland Basin: Subunit IIa – IIc from deepest to shallowest. Subunit IIa generally displays a highly variable and chaotic internal reflection character, with some bright amplitude reflections and distinct internal erosion surfaces (Figures 7, 8c). We interpret this seismic character as related to high energy and dominantly mass-wasted deposition (cf. Donda et al., 2008). In Profile 2 (Figure 7), Subunit IIa is ~0.5 s TWT thick in the southeast but thins out near km 35 against the southeast flank of the dome-structure defined by the IMU surface (Figure 7; km 35). The thinning is partly due to shelfward onlap of internal reflections against the IMU and partly due to truncation of internal, seaward-dipping reflections against the base of the overlying Subunit IIb. Hence, unlike the syn-rift character of Unit I against the BSF, Subunit IIa was not deposited during fault-controlled subsidence, but rather reflects a phase of passive infill during relative uplift towards the NE Greenland margin. This is further indicated by the pronounced seaward tilt of the underlying Unit I and the IMU in Profile 2 (Figure 7). A similar seaward tilt of Unit I and the IMU is observed in the Greenland Basin-part of the parallel Profile 1 further south (Figure 6). Noteworthy, the IMU defines a distinct dome-structure within the COT of Profile 2 (Figure 7; km 35). The dome is about 20 km wide and 0.2 s TWT high, and numerous, almost vertical, faults dissect Unit I below the dome. The faults are seen to offset the IMU as well as the lower layers of Unit II immediately above the IMU. We suggest the dome-structure and the associated faulting are results of a mild compressional phase in relation to the middle-to-upper Miocene IMU. Similar (early to middle Miocene) dome-structures – or low-amplitude folds – are identified, e.g., on the Norwegian margin and in the Faroe-Shetland Basin (Figure 1) and interpreted as evidence of mild compression (Mosar et al., 2002; Løseth and Henriksen, 2005; Doré et al., 2008; Lundin and Doré, 2002; 2011).

In Profile 3 (Figure 8), Subunit IIa of the Greenland Basin displays an overall constant thickness of 0.5 s TWT to the south of the basement mound at km 45. However, northwards from here it thins to less than 0.1 s TWT against the GFZ-EGR. The thinning is mainly associated with apparent, northwards-directed downlap of internal reflections onto the IMU (Figure 8c). We interpret this pattern as evidence of a complete halt in fault-controlled syn-

deposition against the GFZ, that is, the IMU of the Greenland Basin (Figures 7 and 8) defines a pronounced change from low energy sedimentation and syn-rift deposition of Unit I against the BSF and the GFZ to high energy sedimentation and a halt in fault-controlled syn-deposition of Subunit IIa of Unit II.

The uppermost Subunits IIb and IIc of the Greenland Basin are defined by semi-continuous to continuous reflections, with some degree of chaotic reflection pattern but predominantly smaller-scale structures than in Subunit IIa (Figures 7, 8c). The small-scale, chaotic internal reflection character is particularly observed in Subunit IIb and toward the outer shelf slope in Profile 2 (Figure 7; km 20 – 60). Further seaward, internal reflections of Subunit IIb are semi-continuous, sub-parallel and sub-horizontal. We interpret the seismic character of Subunit IIb as a gradual return to overall subtle, deep-marine deposition but with some input of mass-wasted material into the Greenland Basin near the shelf. However, the upper part of the overlying Subunit IIc is characterized by a well-defined, continuous and aggrading reflection pattern (Figures 7b), indicating dominantly bottom current deposition.

Subunits IIb and IIc are both defined by overall constant thicknesses and parallel reflections along Profile 2 (Figure 7). The reflections terminate against the BSF by reflection onlap and indicate passive infill against the fault. A similar reflection pattern is observed for the two subunits in the southern part of Profile 3 (Figure 8b). Here, the subunits each display fairly constant thicknesses of about 2.0 s TWT to the south of km 45. However, north of here they thicken into distinct wedge-shape accumulations, with a total thickness of 1.0 s TWT against the GFZ-EGR. The wedge-shaped geometries contain diverging reflections toward the GFZ, mainly in Subunit IIb and in the lowermost part of Subunit IIc. We interpret this reflection character as renewed syn-rift deposition against the GFZ. The uppermost part of Subunit IIc, however, retrieves the well-defined, continuous and horizontal reflection character as observed in Profile 2 and interpreted as passive infill.

Noteworthy, two, 5 – 10 km wide and up to 0.6 s TWT high, buried basement mounds are observed within the fracture-zone-slope of Profile 3 at km 45 and km 20 (Figure 8b). While Subunit Ia of Unit I is protruded by the basement mounds, Subunit Ib simply appears to be deformed by the mounds and drape them almost without changing its thickness. In contrast, internal reflections of Subunit IIa above the IMU show progressive onlap towards the basement mounds, both from the north and south (Figure 8c). The effect of the basement mounds is not observed in the younger Subunits IIb and IIc. We therefore interpret the two basement mounds as possible buried volcanoes, formed during deposition of Subunit IIa.

5.2. The Greenland Fracture Zone Basin Province (GFZBP)

From the GFZ and northwards (Figures 8b, 9), the seismic basement rises over a distance of ~12 km from 7.5 s TWT in the Greenland Basin to 3.4 – 3.0 s TWT at the crest of the EGR. North of here, basement then deepens, by down-faulting, into the GFZBP, where basement is located as deep as 7.5 s TWT. The GFZBP is bounded to the south and north by opposite-dipping normal faults that define the transitions to less deep basement beneath the EGR and beneath the southern Boreas Basin. In Profile 3 (Figure 8b) this transition is defined by several down-stepping faults, whereas in Profile 4 (Figure 9b) the GFZBP is confined entirely by two steep, opposite-dipping faults, with throws of more than 3 s TWT. Interpretation of Bouguer anomaly data (Døssing et al., 2008) and seismic reflection data (Berger and Jokat, 2009) suggest the GFZBP continues to the northwest of Profile 3 as an elongated, 30 – 50 km wide basin (Figure 3). Here, it is bounded to the southwest by a sheared part of the NE Greenland shelf composed by the GFZ (Døssing and Funck, 2012). Seismic refraction studies further indicate that the EGR and the GFZBP are both seated within highly extended continental crust (Døssing et al., 2008; Døssing and Funck, 2012; Gerlings et al., 2014).

The acoustic basement of the GFZBP is overlain by an up to 3.2 s TWT thick sedimentary succession (Figures 8, 9). Unfortunately, the elevated EGR prohibits direct seismic correlation between Units I and II of the Greenland Basin with layers of the GFZBP. However, the prominent reflector marked as the IMU in the GFZBP (Figures 8c, 9b) corresponds to the regional IMU surface that was mapped by Berger and Jokat (2009) along the outer NE Greenland shelf and throughout the Boreas and Molloy basins (Section 4). However, further correlation of sub-ordinary seismic layers of the GFZBP with identified subunits of the Greenland Basin is less certain. Here, we provide a tentative correlation, based on the assumption that any significant tectonic event or change in stress regime that has affected the Greenland Basin must have affected the GFZBP also.

The pre-IMU succession of the GFZBP can be divided into three layers, based on the identification of two distinct angular unconformities below the IMU (Figures 8b, 9b). We suggest the upper two layers correlate with Subunits Ia and Ib of the Cenozoic Greenland Basin, while sediments below Subunit Ia of the continental GFZBP probably reflect a Mesozoic pull-apart basin that formed during a pre-breakup, intra-continental wrench phase (Døssing et al. 2008; Døssing et al. 2010), that is, the lowermost sediments of the GFZBP probably predate the formation of oceanic crust in the Greenland Basin. Seismic reflections

of this inferred Mesozoic layer further show angular truncation against the base of Subunit Ia, which may reflect an unconformity surface related to breakup of the Greenland Basin. We refer to the inferred Mesozoic layer as Unit M.

Subunits Ia and Ib of the GFZBP are identified in both Profiles 3 and 4 (Figures 8b, 9b). While Subunit Ia is up to 0.4 s TWT thick and defined by relatively bright amplitude reflections, Subunit Ib, immediately below the IMU, is up to 1.0 s TWT thick and appears overall seismically transparent. Subunit Ib as well as the IMU are furthermore heavily dissected by minor, almost vertical reverse faults (Figures 8d, 9c). The faults appear to originate within Subunit Ib and terminate in the layer immediately above the IMU. We suggest the dense reverse fault pattern reflects fluid escape processes from rapidly deposited marine sediments (Gay and Berndt, 2007; Hustoft et al., 2007; Nielsen et al., 2008). No differential thickening is observed of Subunit Ib across the faults.

Subunits Ia and Ib of the GFZBP are characterized by wedge-shaped geometries and diverging reflections toward their bounding faults (Figures 8, 9). This seismic character is similar to Subunits Ia and Ib of the Greenland Basin, interpreted as syn-sedimentary infill of fault-controlled basins (Section 5.1). We suggest the syn-rift character of Subunit Ib, which indicates renewed extension after deposition of Subunit Ia, reflect the early to late Oligocene regional plate reorganizations (Section 2) which caused severe extension across the GFZ (Figure 4b).

In the GFZBP of Profile 3 (Figure 8b), the distinct wedge-shaped geometry of Subunit Ib is controlled mainly by a north-dipping fault along the EGR. The overlying IMU displays a distinct up dip toward and partly over the EGR in this profile. In Profile 4 (Figure 9b), however, Subunit Ib is bounded entirely by the two, opposite-dipping and steep faults of the GFZBP. Here, the IMU displays a broad convex shape, about 0.2 s TWT high. Internal, upper reflections of Subunit Ib are parallel to this surface. A similar, although less distinct, convex shape is observed of the IMU in Profile 3 (Figure 8d; km 20 – 60). We suggest the convex shapes of the IMU in the GFZBP reflect mild compression, similar to what was interpreted for the IMU dome-structure in Profile 2, south of the GFZ (Section 5.1). The fact that upper reflections of Subunit Ib are parallel with the deformed IMU surface in the GFZBP and that the dense reverse faulting of Subunit Ib (fluid escape structures) terminates in the lowermost part of Unit II above the IMU indicate the reverse faulting took place shortly after – or during formation – of the IMU. Hence, it is plausible that both the dome-shaped geometry of the IMU in the GFZBP as well as the fluid escape structures were results of the mild compressional phase, affecting also the IMU to the south of the GFZ.

Unit II of the GFZBP is ~0.4 s TWT thick (Figures 8d, 9c). It is characterized by a well-defined, continuous, prograding to aggrading reflection pattern and has previously been interpreted as a contourite deposit (Nielsen et al., 2008), that is, Unit II of the GFZBP indicates that intensified bottom-water currents controlled deposition north of the GFZ-EGR shortly after the formation of the IMU. We identify three layers in Unit II of the GFZBP, based on identification of two angular unconformities above the IMU. We tentatively suggest these layers correlate with Subunits IIa, IIb and IIc of the Greenland Basin.

In Profile 3 (Figure 8b), Subunit IIa of the GFZBP drapes the deeper part of the EGR, whereas it is entirely confined within the GFZBP in Profile 4 (Figure 9b). We observe no evidence of differential thickening of Subunit IIa across the large bounding faults of the GFZBP. Moreover, internal reflections of Subunit IIa are overall parallel to the IMU and interpreted as passive infill. Thus, the IMU of the GFZBP marks a change from syn-rift deposition of Unit I to overall passive basin infill during deposition of Subunit IIa of Unit II. This change in fault behavior across the IMU is similar to what characterizes the IMU in the Greenland Basin, south of the GFZ (Section 5.1).

Internal upper reflections of Subunit IIa in the GFZBP show angular truncation against the base of Subunit IIc toward the EGR (Figure 8d). Reflections in the lower part of Subunit IIc terminate against this tilted, truncated surface by onlap (Figure 8b). Similarly, Subunit IIb pinches out toward the EGR (Figures 8b, 9b) by reflection onlap against Subunit IIa. We suggest these observations indicate two phases of footwall uplift over the EGR during deposition of Subunit IIb and of the lower part of Subunit IIc. The uplift of EGR may have been caused by unloading of the EGR by coincident syn-rift deposition of Subunits IIb and IIc in the Greenland Basin against the southwards-dipping fault of the GFZ (Section 5.1). We note that several normal faults offset the seabed as well as Subunit IIa and the upper part of Subunit IIc over the crest of the EGR (Figure 8b). However, we observe no differential thickening of these subunits across the faults. This indicates that faulting took place during deposition of Subunit IIb and the lower part of Subunit IIc, that is, during footwall uplift of the EGR and deposition of Subunit IIb and Subunit IIc in the GFZBP.

5.3. Tectonic subsidence history of the Greenland Basin against the GFZ transform margin

In order to evaluate the thermo-mechanical evolution of the GFZ and, thus, the tectonic subsidence history of the Greenland Basin lithosphere against the GFZ, we have carried out some 2-D backstripping calculations of seismic layers identified in the Greenland Basin-part

of Profile 3 (Figure 8b). For this we applied a regional model of isostatic compensation (flexural isostasy). The modeling included the following calculations: (1) Time-to-depth conversion of sedimentary layers, using the seismic velocity model of Døssing et al. (2008), (2) 2-D modelling of oceanic basement flexure to obtain a best fit estimate of the mean elastic thickness of the lithosphere, $T_{e(best)}$, and (3) 2-D flexural backstripping of the sedimentary layers, with $T_{e(best)}$ as input.

5.3.1. 2-D flexure modeling

We have modelled the flexure with a semi-infinite, broken plate that overlies an inviscid fluid. The plate break was assumed to be located at a south-dipping normal fault at the GFZ. As pointed out by Heiskanen and Vening Meinesz (1958), the crust on the hanging wall side of a normal fault is loaded by an additional, triangular-shaped load, causing subsidence. In contrast, the footwall side is unloaded, causing uplift. The Greenland Basin is located on the hanging wall so we calculated the additional load from the fault geometry, i.e. the dip, θ, and depth of faulting, h_0 (Watts, 2001, p. 291 – 292). We assumed an initial fault dip of 45°, consistent with the velocity model of Døssing et al. (2008). The flexure was then calculated using a finite difference technique (Bodine et al., 1981) in which the fault is simulated by T_e = 0 km.

Figure 10 shows the results of the 2-D flexural modeling of the Greenland Basin basement surface of Profile 3. By comparing the calculated basement flexure models, using different values of the mean elastic thickness (T_e) and depth of faulting (h_0) with the observed basement surface, we obtain a best fit model, $T_{e\,(best)}$, of 10 km for h_0 of 16 km. Lower T_e-values (e.g., T_e = 7 km) produce too narrow and deep a basin, while higher values (e.g., T_e = 14 km) produce too wide and shallow a basin. We found that changing θ and h_0 and, thus, the fault geometry which determines the size of the load acting at the GFZ had little effect on these conclusions. Maximum curvature (Figure 10) of the flexure was found by differentiating the best fit curve and is located near the interpreted volcanic basement mound at km 45.

If we assume that T_e is given by the depth of the 450°C oceanic isotherm, then the expected T_e for the early Eocene (~50 Ma) oceanic lithosphere along Profile 3 is about 20 km (cf. Watts, 2001). Looking strictly at oceanic lithosphere near fracture zones, however, the expected T_e tend to follow the depth of the 600°C oceanic isotherm (Watts, 2001), that is, T_e is expected to be ~25 km for ~50 Ma crust. The expected T_e-values of 20–25 km are significantly greater than our preferred $T_{e\,(best)}$ of 10 km (Figure 10). We suggest the low T_e

might be related to intense yielding, through brittle and ductile deformation in the flexed lithosphere beneath the GFZ trench slope. Evidence of possible pronounced brittle deformation along the GFZ trench slope is shown in Supplementary Material Figure S4.

Alternatively, thermal resetting of the early Eocene Greenland Basin lithosphere at a later stage might also have lowered its elastic thickness. Thus, a $T_{e\ (best)}$ of 10 km is expected to correlate with a crustal age of ~10 – 20 Ma according to the 450°C and 600°C oceanic isotherms (Watts, 2001), that is, oceanic lithosphere in Profile 3 might have been affected by a thermal resetting at some time during the Miocene. If this is the case, we tentatively suggest this thermal event could have been related to the formation of the volcanic basement mounds, interpreted to be of middle-to-late Miocene age (Figure 8b; Section 5.1).

5.3.2. 2-D flexural backstripping and tectonic subsidence analysis

Kinematic models of transform margins, such as the GFZ-EGR-GFZBP (Figure 3), normally distinguish between four phases in their tectonic development (Mascle and Blarez, 1987). During Phase 1, intra-continental wrenching dominates along the future transform zone. We suggest this phase is reflected by the inferred pre-breakup Mesozoic Unit M of the GFZBP (Figure 9; Section 5.2). Seafloor spreading then normally initiates during Phase 2 and culminates in Phase 3 by the passage of an active spreading ridge along the transform (Mascle and Blarez, 1987; Gadd and Scrutton, 1997). In the final Phase 4, the transform margin is expected to become passive (Mascle and Blarez, 1987), that is, plates on either side of the transform move in conjunction and lateral stresses cease. At this stage, the blocks on either side of the fracture zone continue to become cooler and denser and, thus, subside isostatically at different rates due to their different thermal age (Sandwell and Schubert, 1982). Onset of Phase 4 is normally associated with a change in the mechanical behavior of the transform from decoupling to coupling, that is, a shift from differential subsidence accommodated by faulting to differential subsidence without faulting. The coupling results in a localized upward flexure of the younger oceanic lithosphere and downwards flexure of the continental lithosphere in the vicinity of the fracture zone (Wessel and Haxby, 1990; Lorenzo and Wessel, 1997).

While the 2-D forward flexure modeling approach (Figure 10) yields insight into the background T_e structure of the Greenland Basin, it provides little information on the thermos-mechanical history of the GFZ and how the tectonic subsidence against the fracture zone has changed through time. We have therefore backstripped the sedimentary layers that underlie the Greenland Basin in Profile 3 (Figure 8b) progressively through time, assuming 2-D

flexural isostasy with T_e of 10 km (cf. Figure 10) and a plate break at the GFZ. The results provide the depth that basement would be in the absence of sediment loads. We are aware that a T_e of 10 km in the flexural backstripping gives us the accumulative flexure of oceanic lithosphere towards the GFZ, and although lower than expected for the lithospheric age, it appears reasonable given the amount of curvature and yielding that has occurred.

Figure 11 shows the results of our flexural backstripping after removing Subunits Ia, Ib, IIa – IIc of the Greenland Basin. The resulting basement depths indicate the tectonic subsidence of the Greenland Basin-lithosphere against the GFZ at each stage and, hence, the thermo-mechanical evolution of the GFZ. Subunit Ia (Figure 11b) was deposited directly on oceanic crust in the Greenland Basin. It therefore represents the expected Phase 2 of Mascle and Blarez (1987) in which nascent oceanic lithosphere and continental lithosphere are juxtaposed, being separated by a mechanically decoupled transform fault. The mechanical decoupling is supported by the depression adjacent to the GFZ in the backstrip for Subunit Ia (Figure 11b) and by the syn-rift seismic character of the subunit (Section 5.1). The overlying Subunit Ib (Figure 11c) ideally represents Phase 3 of Mascle and Blarez (1987). However, according to plate models (Figure 4) the GFZ-EGR-GFZBP transform margin was never affected by the passing of an active spreading ridge to the south. Instead, early to late Oligocene (chron C13 – C7) plate reorganizations (Srivastava and Tapscott, 1986) imposed severe extension across the GFZ-EGR-GFZBP and ultimately caused the separation of the EGR from the paleo-Barents Sea margin. Thus, the depression adjacent to the GFZ in the backstrip for Subunit Ib (Figure 11c) and the seismic syn-rift character of the subunit reflect continued mechanical decoupling of the GFZ during this phase.

We compute a localized upward flexure towards the GFZ in the backstrip for Subunit IIa (Figure 11d), which indicates deposition during mechanical coupling of the GFZ. This result correlates well with the seismic character of Subunit IIa, which indicates a complete halt in fault-controlled subsidence against the GFZ (Section 5.1). By restoring the present-day, apparent reflection downlap pattern of Subunit IIa (Figure 8c) to its backstrip surface, we find the present-day downlap pattern was originally deposited as an onlap pattern towards the GFZ (Figure 11d - inset). This result is further supported by also restoring the dipping flanks of the internal buried erosional channels of Subunit IIa (Figure 8c) to the backstrip surface, which makes them horizontal as expected. The restored onlap reflection pattern of Subunit IIa onto the underlying IMU surface (Figure 11d - inset) closely resembles that of oceanic sedimentary layers deposited against a transform margin during thermo-mechanical coupling (Wessel and Haxby, 1990; Lorenzo and Wessel, 1997; Clift et al., 1997).

The final backstrip surfaces for Subunit IIb (Figure 11e) and Subunit IIc (Figure 11f) show depressions against the GFZ, indicating renewed mechanical decoupling after the deposition of Subunit IIa. This interpretation is supported by the overall seismic syn-rift character of the two subunits near the GFZ (cf Section 5.1). We suggest the renewed decoupling relates to Pliocene and younger (that is, after deposition of the middle-to-late Miocene Subunit IIa) plate adjustments along the Mohns and Knipovich ridges (cf. Crane et al., 2001; Demets et al., 2010).

We summarize our interpretation of the tectonic subsidence history of the Greenland Basin against the GFZ in Figure 12.

6. DISCUSSION

6.1. The IMU event

The seismic results from the GFZ-area (Døssing et al., this study) document that the IMU reflects a key tectono-stratigraphic event in the deep-sea off the NE Greenland shelf. Our preferred age of this event is middle-to-late Miocene (Section 4). We show that the IMU marks: (i) a change from thermo-mechanical de-coupling to coupling across the GFZ, (ii) widespread termination of syn-rift deposition, e.g., in the COT along the outer NE Greenland margin to the south of the GFZ and in the GFZBP to the north of the GFZ (Figure 3), (iii) the onset of mild compression in the COT and possibly in the GFZBP, and (iv) the onset of contourite deposition in the GFZBP, north of the GFZ. Significantly, previous seismic results from the adjacent NE Greenland shelf (Figure 6) (Hamann et al. (2005; Berger and Jokat, 2008; 2009) show that the IMU further defines the onset of pronounced margin-wide continental tilting in NE Greenland, with uplift of the inner margin and massive eastward outer-shelf progradation, as well as widespread mild compression (Hamann et al., 2005). Based on the seismic results (Døssing et al., this study), we show that the eastward shelf progradation during the Miocene provided surplus material for the adjoining Greenland Basin, changing its depositional environment from subtle hemipelagic deposition of Unit I below the IMU to high-energy mass-wasting of Subunit IIa above the IMU.

6.2. Ridge relocations along the Mohns and Knipovich ridges at the IMU event

The synchroneity of the NE Greenland margin uplift and widespread mild basin compression at the IMU event indicates a common tectonic mechanism that involves – or is driven by – compressional shortening. Significantly, the onset of thermo-mechanical coupling

across the GFZ (and the general termination of syn-rift deposition in the study area) strongly indicates that the IMU event was directly related to plate kinematic changes along the Mohns and Knipovich ridges, separated by the GFZ (Figure 3).

Magnetic spreading anomalies are well-defined along the Mohns Ridge (Figure 5), while anomalies in the Boreas Basin, north of the GFZ-EGR, and along the Knipovich Ridge are generally of low amplitude, discontinuous and ambiguous. The disturbed magnetic pattern to the north of the GFZ probably relates to the combination of a highly sheared rifting history (Faleide et al., 1993; Døssing et al., 2010), multiple readjustments of the plate boundaries (Crane et al., 2001; Mosar et al., 2002; Engen et al., 2008), locally thick sediments (Berger and Jokat, 2009) and isolated components of highly extended, weakly magnetic continental crust or partially serpentized mantle (Døssing et al., 2008; Hermann and Jokat, 2013; Gerlings et al., 2014).

Oceanic crust has been inferred in several studies in the Boreas Basin, although the various studies strongly disagree on the age and plate kinematic evolution of this basin (e.g., Mosar et al., 2002; Breivik et al., 2003; Engen et al., 2008; Ehlers and Jokat, 2009; Libak et al., 2012). Based on a basin-wide seismic reflection profile, helicopter borne magnetic data and a basement roughness study, Ehlers and Jokat (2009) could confirm an ultraslow environment and suggest seafloor spreading initiated at chron C9 time in the middle of the Boreas Basin. Seismic refraction data from the southern Boreas Basin, however, indicate crustal velocities that could either be interpreted as highly extended continental crust or partially serpentinized mantle (Gerlings et al., 2014). Thus, the formation and crustal setting of the older Boreas Basin as a whole is complex and probably not fully resolved.

Anomalies C6 (~19.5 Ma; late early Miocene) to C5 (~10.5 Ma; late Miocene) appear to define the first clear spreading anomalies, traceable along the entire the Knipovich Ridge (Figure 5). According to Engen et al. (2008), anomaly C6 is the first spreading anomaly that can also be traced across the projected fault trace of the GFZ and, hence, may define the formation of a continuous plate boundary along the Mohns and Knipovich ridges. Anomaly C5, on the other hand, appears to be the first well developed magnetic anomaly that extends along all spreading segments between the northern NE Atlantic and the Arctic Ocean (Engen et al., 2008). This anomaly also has a regular shape compared to anomaly C6, which according to Engen indicates that onset of the present-day mode of seafloor spreading, including opening of the Fram Strait corridor (Figure 1), may have been delayed until C5

times. Mosar et al. (2002), however, suggest that anomaly C5 defines both the merging of the Mohns and Knipovich as well as the onset of the present-day mode of seafloor spreading.

We suggest that the preferred middle-to-late Miocene age (~15–10 Ma) of the IMU event (Section 4) and, in particular, the coincident thermo-mechanical coupling across the GFZ (Section 5.1) place direct temporal and tectonic constraints on an important event along the Mohns and Knipovich ridges (Figure 3), specifically the formation of a continuous (modern) plate boundary. Thus, the formation of a continuous plate boundary along the Mohns and Knipovich ridges would imply that plates on either side of the GFZ started to move in conjunction, thereby causing differential stresses to cease. This, in turn, would facilitate the onset of thermo-mechanical coupling across the fracture zone (cf. Maszle and Blarez, 1987). Such an event may further explain the widespread termination of syn-rift deposition observed in the study area.

The formation of a continuous plate boundary is supported by the presence of contourite deposits above the IMU in the GFZBP (Section 5.2). We attribute these to intensified bottom currents in the southern Boreas Basin, and suggest they reflect a significant widening of the Fram Strait corridor as promoted by the interpreted ridge relocations along the Mohns and Knipovich ridges. Previously proposed ages of a significant widening of the Fram Strait vary from late early to late Miocene (Winkler et al., 2002; Jakobsson et al., 2007; Engen et al., 2008; Knies and Gaina, 2008; Ehlers and Jokat, 2013). We summarize our view of the regional plate tectonic setting – prior to and shortly after the IMU event – in Figure 13.

6.3. The IMU and phases of uplift in the NE Atlantic

The middle to late Miocene age (~15–10 Ma) of the IMU event overlaps with an interpreted late Miocene (~10 Ma) event of pronounced surface uplift in central West Greenland and in southern and central East Greenland, within the uncertainty of the methods applied (Thomson et al., 1999; Japsen et al., 2006, 2014). Likewise, the Barents Sea and Svalbard on the European side of the NE Atlantic appear to have been affected by late Miocene vertical motion (Vågnes and Amundsen, 1993; Green and Duddy, 2010, Dörr et al., 2013). Late Miocene uplift may also have affected areas farther from our study area, for example the American Cordillera (Farley et al., 2001; Reiners et al., 2002; Foster et al., 2010). The IMU event further overlaps with intra-Miocene and middle Miocene

unconformities, identified in deep-water basins and on basin margins, e.g., in the Faroe-Shetland area (Andersen et al., 2000) and on the Norwegian margin (Brekke, 2000) and inferred to relate to tectonic movements (Stoker et al., 2005). These unconformities are often associated with evidence of early to middle Miocene compressional doming (Figure 1) (Lundin and Doré, 2002; Doré et al., 2008). In contrast, the onset of Neogene uplift and exhumation around southern Scandinavia appears to have occurred in the earliest Miocene (Stoker et al., 2005; Japsen et al., 2007, 2015; Rasmussen, 2009).

The question is whether the plate kinematic changes along the Mohns and Knipovich ridges at the time of the IMU event were responsible not only for the onset of thermo-mechanical coupling across the GFZ and the widespread termination of syn-rift deposition, but also were directly responsible for the coincident middle-to-late Miocene margin uplift and mild compression in NE Greenland – and the Miocene tectonic events elsewhere in the NE Atlantic? Or if the regional plate kinematic changes and the margin uplift were simply effects of global plate-motion events or of underlying mantle dynamics, e.g., related to the Iceland plume (Figure 1)?

6.4. Role of the Iceland plume and plate forces

Seismic models of P- and S-wave anomalies clearly image a thick, sub-lithospheric, low-velocity layer beneath Iceland, indicative of a mantle plume (Wolfe et al., 1997; Bijwaard and Spakman, 1999). Investigations of S-wave data (Weidle and Maupin, 2008; Rickers et al., 2013) further indicate that the low-velocity layer extends beneath oceanic crust of the NE Atlantic and beneath the rifted continental margins of eastern Greenland, the western British Isles and southern Scandinavia. Here, it largely correlates spatially with the regions of highest topography (Arrowsmith et al., 2005; Medhus et al, 2012; Steinberger et al., 2015). A residual topography model of the NE Atlantic (Jones et al., 2014) supports a regional extent of the Iceland plume head, with a wavelength of more than 1000 km, that is, the present-day topography of the NE Atlantic and its continental margins appears to have some degree of regional dynamic support from underlying anomalously hot mantle.

Studies of V-shaped ridges, south of Iceland, document a distinctive pulsating nature of the Iceland plume (Ito, 2001; Jones et al., 2002; 2014; Poore et al., 2009). By relating mantle potential temperature (T_p) to oceanic crustal thickness variations (Parkin and White, 2008) and, hence residual depth, Parnell-Turner et al. (2014) were able to map changes in the

periodicity and amplitude of the pulses since 55 Ma (Figure 14). Between 55 and 35 Ma, they find only small fluctuations in mantle temperature (5–10 °C) and a periodicity of ~3 Myr. Since then, the plume head has expanded and its periodicity has changed to about 8 Myr, reflecting changes in mantle temperature of 25–30 °C. By closely inspecting the curve of Parnell-Turner et al. (2014), however, it appears that their interpreted transition at 35 Ma was preceded by a sharp and high-amplitude increase in T_p of more than 30°C, starting around 40 Ma (Figure 14). Similar increases in the mantle temperature appear to have taken place between 20 Ma and 15 Ma and again between 7 Ma and 5 Ma (Parnell-Turner, pers. comm., 2015); each event preceded by a period with overall gently decreasing mantle temperatures. The three sharp and high-amplitude increases in T_p roughly correlates with similar increases in crustal production rates, found by analyses of deep-seismic data along NE Atlantic spreading ridges immediately to the north of Iceland (Mjelde and Faleide, 2009). Here, Mjelde and Faleide (2009) find evidence of marked increases in the crustal production rates (interpreted by Mjelde and Faleide as increases in volume flux of the Iceland plume) around 23 Ma and 10 Ma as well as a minor increase around 40 Ma (Figure 14 – lower plot). Hence, based on Figure 14, the Iceland plume appears to have had periods of sharp increases in mantle temperature (i.e. hot pulses) from c. 40–35 Ma and again from c. 23–15 Ma and c. 10–7 Ma. Such pulses of anomalously hot mantle that spread out radially from Iceland and beneath the lithospheric plates have been suggested to drive transient uplift events (White and Lovell, 1997; Jones and White, 2003; Rudge et al., 2008; Shaw Champion et al., 2008; Hartley et al., 2011) as well as margin compressional events (Doré et al., 2008; cf. Figure 1). However, due to the finite velocity of a hot pulse and the distance to the NE Greenland margin, the travel-time delay of a hot pulse originating at the Iceland plume center has to be taken into account before we can try to link individual plume pulses or changes in the pulsating behavior with the IMU event.

From comparative analyses of basin uplift events on the NW European margin and in the North Sea, Hartley et al. (2011) estimate a radial velocity of ~35 cm/yr of hot pulses from the plume beneath the lithospheric plate. This estimate is roughly similar to other estimates, based on direct observations of V-shaped ridges (Poore et al., 2009; 2011; Walters et al., 2013; Parnell-Turner et al., 2015). At present, the NE Greenland margin is located c. 900–1,300 km from the plume center (Torsvik and Cocks, 2005). If we consider the three hot pulses around 40–35 Ma, 23–15 Ma and 10–7 Ma (Figure 14) as the most likely candidates for inducing uplift in NE Greenland at the IMU event, we can correct for a northwestwards

motion of the Greenland plate over the mantle (Steinberger et al., 2015) subsequent to these events of ~4.0°, ~1.0° and ~0.5°, respectively (northward components). The present-day distance thereby reduces to ~650 km at 40–35 Ma, ~950 km at 23–15 Ma and ~1050 km at 10–7 Ma. Assuming a radial velocity of around 35 cm/yr, the hot pulse that spread out from the Iceland plume center at c. 40–35 Ma would arrive beneath the NE Greenland margin around 38–33 Ma, that is, long before the middle-to-late Miocene (~15–10 Ma) IMU event. On the other hand, the hot pulse at c. 10–7 Ma would arrive after the IMU event, around 7–4 Ma. However, the hot pulse at c. 23–15 Ma (Figure 14) would arrive around 20–12 Ma in NE Greenland. It may therefore be a possible candidate for the cause of the IMU event. Considering the effect of the Iceland plume on the NE Atlantic spreading system in general (e.g., Mosar et al., 2002) it is plausible that such a prominent hot pulse event could have affected the Miocene plate kinematics along the Mohns and Knipovich ridges and thereby facilitated the onset of coupling across the GFZ. A marked increase in mantle temperatures along the spreading ridges may further explain the observations of mild compression in the study area as a result of increased ridge push. This has been proposed to be the cause for compressional structures which are located closer to Iceland (Figure 1) and are of mainly early Miocene (Doré et al., 2008), that is, within the age range of the hot pulse at c. 23–15 Ma.

However, if the IMU event in NE Greenland was part of the pronounced late Miocene (~10 Ma) surface uplift in East and West Greenland (Thompson et al., 1999; Japsen et al., 2006; 2014), the role of the Iceland plume as the driving mechanism behind the IMU event may be questioned. The magnitude of the late Miocene surface uplift has been estimated to be equal (~1 km) in both West and East Greenland, whereas the magnitude of a subsequent early Pliocene event of uplift has been estimated to ~2 km in East Greenland but only ~1 km in West Greenland. This asymmetry in Pliocene uplift may have created the higher mountains in East Greenland (<3.7 km a.s.l.) compared with West Greenland (<2 km a.s.l.) (Japsen et al., 2014). Given the proximity of East Greenland to Iceland (<500 km; Figure 1), Japsen et al. (2014) therefore speculate that this excess elevation is related to enhanced dynamic support by the Iceland plume since about 5 Ma. According to this argument, one would expect the Miocene IMU event to be asymmetric across Greenland if being caused by a hot pulse from Iceland. This does not appear to the case (Thomson et al., 1999; Japsen et al., 2006, 2014). However, given the uncertainty of the methods applied, we cannot rule out the Iceland plume as the driving mechanism for the IMU event.

Alternatively, the possible synchroneity of the middle-to-late Miocene IMU event with phases of uplift, found in East and West Greenland (and elsewhere) may point to changes in global tectonics and intra-plate stresses as the cause of uplift and plate-motion changes. Based on previously unpublished magnetic data, Merkouriev and DeMets (2008) and subsequently Iaffaldano and Bunge (2015) confirmed a previously undetected rapid spreading reduction in the NE Atlantic in the late Miocene. These results contradict previous results from the NE Atlantic which suggest fairly constant spreading rates since ~20 Ma (Mosar et al., 2002; Torsvik and Cocks, 2005). The spreading rate of a modern ridge mirrors its status in the global plate tectonics (Husson et al., 2015), and studies of global seafloor generation rates (Cogné and Hummel, 2006) show that significant changes took place during the late Miocene. We therefore speculate that an increase in compressional stresses enforced the drop in NE Atlantic spreading rates during the late Miocene, leading to uplift and mild compression on the NE Greenland margin – and possibly elsewhere in the NE Atlantic, including West and East Greenland (where km-scale uplift has been suggested to begin in the late Miocene; Japsen et al., 2006, 2014). A change in intra-plate stresses may further explain the plate-motion changes along the Mohns-Knipovich ridges at the time of the IMU event.

The seismic results presented in this study document that the IMU event of surface uplift and mild compression in NE Greenland was directly related to plate-motion changes across the GFZ and, thus, along the Mohns and Knipovich ridges, at some time during the middle-to-late Miocene. The correlation between margin uplift and plate-motion changes indicates a direct causality between margin uplift and plate tectonic forces. Considering the middle-to-late Miocene age of the IMU event and the proximity of eastern Greenland to Iceland, these forces may relate to enhanced dynamic support from a hot pulse from the Iceland plume and/or to changes in intra-plate stresses related to global tectonics. Obtaining a more precise age of the IMU event is critical in order to fully investigate its origin and its correlation with other events of margin uplift and compression in the NE Atlantic. Furthermore, a better understanding of the interaction between horizontal and vertical forces along passive margins awaits further global studies of coupled models of the mantle/lithosphere system (Iaffaldano and Bunge, 2009, 2015).

7. CONCLUSIONS

A regional, angular unconformity of Miocene age (Intra Miocene Unconformity, IMU) on the NE Greenland shelf defines the base of a major, eastward prograding shelf sequence that

reflects the onset of pronounced inner margin uplift, combined with glacial erosion and successive advances of the Greenland ice-sheet onto the shelf. Seismic-to-borehole ties to ODP-sites 909 and 913 constrains the age of the IMU to middle-to-late Miocene (~15 – 10 Ma).

Based on previously published and unpublished seismic reflection profiles, we trace the IMU across the GFZ-EGR, located in the deep-sea off the NE Greenland shelf. We demonstrate that the IMU defines a change from thermo-mechanical decoupling to coupling across the GFZ as well as a general termination of syn-rift deposition in the area. We relate these changes to a cease in lithospheric extensional stresses induced by important ridge relocations along the Mohns and Knipovich ridges; more specifically by the formation of a continuous plate boundary along the Mohns-Knipovich spreading ridges and a plate-kinematic bypassing of the GFZ. We further show that the IMU is associated with widespread mild compression in highly extended continental basins. Our results imply a direct causality between pronounced Miocene uplift in NE Greenland, mild basin compression and plate-motion changes in the NE Atlantic.

We demonstrate that the IMU event marks the onset of contourite deposition in basins immediately to the north of the GFZ-EGR. We interpret the contourite deposition as evidence of intensified bottom currents related to an accelerated widening of the Fram Strait. This widening was probably caused by the concurrent plate-motion changes along the Mohns and Knipovich ridges and minor spreading segments further north

The correlation between margin uplift and plate-motion changes found in this study indicates a direct causality between margin uplift and plate tectonic forces. Based on the estimated middle-to-late Miocene age of the IMU event and the proximity of eastern Greenland to Iceland, we speculate that the these forces may relate to enhanced dynamic support from a hot pulse from the Iceland plume and/or to changes in intra-plate stresses related to global tectonics. However, obtaining a more precise age of the IMU event is critical in order to fully investigate its origin and its possible correlation with significant events of late Miocene surface uplift found in West and East Greenland

Acknowledgements.

The paper is published with permission from the Geological Survey of Denmark and Greenland. Seismic data to support this article are from the Geological Survey of Denmark and Greenland and the Alfred Wegener Institute. Because of confidentiality issues, the seismic data have not been released. Thanks to John Maclennan (University of Cambridge, UK) and Ross Parnell-Turner (University of Cambridge, UK) for valuable discussions.

REFERENCES

Anell, I., Thybo, H., Artemieva, I.M., 2009. Cenozoic uplift and subsidence in the North Atlantic region: Geological evidence revisited. Tectonophysics 474, 78-105.

Arrowsmith, S. J., Kendall, M., White, N., VanDecar, J. C., and Booth, D. C., 2005. Seismic imaging of a hot upwelling beneath the British Isles. Geology, 33(5), 345-348.

Berger, D., Jokat, W., 2008. A seismic study along the East Greenland margin from 72°N to 77°N. Geophys. J. Int. 174 (2), 733 – 748.

Berger, D., Jokat, W., 2009. Sediment deposition in the northern basins of the North Atlantic and characteristic variations in shelf sedimentation along the East Greenland margin. Mar. Petr. Geol. 26 (8), 1321 – 1331, 10.1016/j.marpetgeo.2009.04.005.

Bijwaard, H. and Spakman, W., 1999. Tomographic evidence for a narrow whole mantle plume below Iceland. Earth Planet. Sci. Lett., 166, 121 – 126.

Bodine, J. H., Steckler, M. S., Watts, A. B., 1981. Observations of flexure and the rheology of the oceanic lithosphere. J. Geophys. Res. 86, 3695-3707.

Bonatti, E., Crane, K., 1982. Oscillatory spreading explanation of anomalously old uplifted crust near oceanic transforms. Nature 300, 343-345.

Bonatti, E., Ligi, M., Gasperini, L., Peyve, A., Raznitsin, Y., Chen, Y., 1994. Transform migration and vertical tectonics at the Romanche fracture zone, equatorial Atlantic. J. Geophys. Res. 99, 21779-21802, doi:10.1029/94JB01178.

Bonow, J. M., Japsen, P. and Nielsen, T.F.D., 2014. High-level landscapes along the margin of southern East Greenland – A record of tectonic uplift and incision after breakup in the NE Atlantic, Global and Planetary Change, 116, 10 – 29.

Bott, M.H.P., 1991. Ridge push and associate plate interior stress in normal and hot spot regions. Tectonophysics, 200, 17 – 32.

Breivik, A.J., Mjelde, R., Grogan, P., Shimamura, H., Murai, Y., and Nishimura, Y. (2003). Crustal structure and transform margin development south of Svalbard based on ocean bottom seismometer data. Tectonophysics, 369(1 – 2), 37 – 70.

Brooks, K., 2011. The East Greenland rifted volcanic margin. Geol. Surv. Den. Green. Bull. 24, 96 pp.

Clift, P. D., Lorenzo, J. M., Carter, A., Hurford, A.J., and ODP Leg 159 Scientific Party, 1997. Transform tectonics and thermal rejuvenation on the Côte d'Ivoire-Ghana margin, west Africa. J. Geol. Soc. Lond. 154(3), 483 – 489.

Cloetingh, S., Gradstein, F.M., Kooi, H., Grant, A.C., and Kaminski, M., 1990. Plate reorganization: a cause of rapid late Neogene subsidence and sedimentation around the North Atlantic? Journal of the Geological Society, 147, 495 – 506.

Cogné, J. P., and Humler, E., 2006. Trends and rhythms in global seafloor generation rate. Geochemistry, Geophysics, Geosystems, 7(3), doi:10.1029/2005GC001148.

Crane, K., Doss, H., Vogt, P., Sundvor, E., Cherkashov, G., Poroshina, I., and Joseph, D., 2001. The role of the Spitsbergen shear zone in determining morphology, segmentation and evolution of the Knipovich Ridge. Marine Geophysical Researche, 2(3), 153 – 205.

Davis, M. W., White, N. J., Priestley, K. F., Baptie, B. J., and Tilmann, F. J., 2012. Crustal structure of the British Isles and its epeirogenic consequences. Geophysical Journal International, 190(2), 705-725.

DeMets, C., Gordon, R. and Argus, D.F., 2010. Geologically current plate motions. Geophys. J. Int., 142, 1 – 80.

Donda, F., O'Brien, P. E., De Santis, L., Rebesco, M., and Brancolini, G., 2008. Mass wasting processes in the Western Wilkes Land margin: possible implications for East Antarctic glacial history. Palaeogeography, Palaeoclimatology, Palaeoecology, 260(1), 77-91.

Doré, A. G., Lundin, E. R., Kusznir, N. J., Pascal, C., 2008. Potential mechanisms for the genesis of Cenozoic domal structures on the NE Atlantic margin: pros, cons and some new ideas. Geol. Soc. Lond. Spec. Publ. 306, 1 – 26.

Doré, A. G. and E.R. Lundin, 1996. Cenozoic compressional structures on the NE Atlantic margin: nature, origin and potential significance for hydrocarbon exploration. Petr. Geoscience, 2, 299 – 311.

Dörr, N., P. D. Clift, F. Lisker, and C. Spiegel, 2013. Why is Svalbard an island? Evidence for two-stage uplift, magmatic underplating, and mantle thermal anomalies. Tectonics 32, no. 3, 473-486.

Døssing, A., Dahl-Jensen, T., Thybo, H., Mjelde, R., Nishimura, Y., 2008. East Greenland Ridge in the North Atlantic Ocean: An integrated geophysical study of a continental sliver in a boundary transform fault setting. J. Geophys. Res. 113 (B10107), doi: 10.1029/2007JB005536.Døssing, A., Stemmerik, L., Dahl-Jensen, T., Schlindwein, V., 2010. Segmentation of the eastern North Greenland oblique-shear margin: regional plate tectonic implications. Earth Plan. Sci. Lett. 292(3 – 4), 239 – 253.

Døssing, A and Funck, T., 2012. Greenland Fracture Zone-East Greenland Ridge(s) revisited: Indications of a C22-change in plate motion? J. Geophys. Res. Solid Earth, 117, B1, doi: 10.1029/2011JB008393.

Ehlers, B.M. and Jokat, W., 2009. Subsidence and crustal roughness of ultra-slow spreading ridges in the northern North Atlantic and the Arctic Ocean. Geophysical J. Int., 177, 451 – 462, doi: 10.1111/j.1365-246X.2009.04078.x.

Ehlers, B.M. and Jokat, W., 2013. Paleo-bathymetry of the northern North Atlantic and consequences for the opening of the Fram Strait. Marine Geophysical Research, 34(1), 25 – 43.

Eidvin, T., Riis, F., and Rasmussen, E. S., 2014. Oligocene to Lower Pliocene deposits of the Norwegian continental shelf, Norwegian Sea, Svalbard, Denmark and their relation to the uplift of Fennoscandia: A synthesis. Marine and Petroleum Geology, 56, 184-221.

Eidvin, T., Jansen, E., Rundberg, Y., Brekke, H. and Grogan, P., 2000. The Upper Cainozoic of the Norwegian continental shelf correlated with the deep sea record of the Norwegian Sea and North Atlantic. Mar. Petrol. Geol., 17, 579-600.

Engen, Ø., Faleide, J. I., Dyreng, T. K., 2008. Opening of the Fram Strait gateway: A review of plate tectonic constraints. Tectonophysics 450 (1 – 4), doi:10.1016/j.tecto.2008.01.002.

Faleide, J. I., Tsikalas, F., Breivik, A. J., Mjelde, R., Ritzmann, O., Engen, Wilson, J. D., Eldholm, O., 2008. Structure and evolution of the continental margin of Norway and the Barents Sea. Episodes 31, 82 – 91.

Faleide, J. I., Vågnes, E., and Gudlaugsson, S. T. (1993). Late Mesozoic-Cenozoic evolution of the south-western Barents Sea in a regional rift-shear tectonic setting. Marine and Petroleum Geology, 10(3), 186-214.

Farley, K.A., Rusmore, M.E., Bogue, S.W., 2001. Post–10 Ma uplift and exhumation of the northern Coast Mountains, British Columbia. Geology 29, 99–102.

Foster, G.L., Lunt, D.J., Parrish, R.R., 2010. Mountain uplift and the glaciation of North America - a sensitivity study. Clim. Past 6, 707–717.

Gadd, S. A., Scrutton, R. A., 1997. A integrated thermomechanical model for the transform continental margin evolution. Geo. Mar. Lett. 17, 21 – 30.

Gaina, C., L. Gernigon, P. Ball, 2009. Palaeocene-Recent plate boundaries in the NE Atlantic and the formation of the Jan Mayen microcontinent. J. Geol. Soc. London, 166, 601 – 616.

Gay, A. and Berndt, C., 2007. Cessation/reactivation of polygonal faulting and effects on fluid flow in the Vøring Basin, Norwegian Margin. Journal of the Geological Society, 164 (1), 129-141, doi:10.1144/0016-76492005-178.

Gerlings, J., T. Funck, C.F. Castro, J.R. Hopper, 2014. The East Greenland Ridge – a continental sliver along the Greenland Fracture Zone. Geophysical Research Abstracts, Vol. 16, EGU2014-2879, 2014. EGU General Assembly 2014

Gernigon, L., Gaina, C., Olesen, O., Ball, P.J., Péron-Pinvidic, G., and Yamasaki, T., 2012. The Norway Basin revisited: From continental breakup to spreading ridge extinction. Marine and Petroleum Geology, 35(1), 1 – 19.

Gradstein, F.M, Ogg, J.G., Schmitz, M.D., et al., 2012, The Geologic Time Scale 2012: Boston, USA, Elsevier, DOI: 10.1016/B978-0-444-59425-9.00004-4.

Green, P. F., and I. R. Duddy, 2010. Synchronous exhumation events around the Arctic including examples from Barents Sea and Alaska North Slope. In *Geological Society, London, Petroleum Geology Conference series*, vol. 7, pp. 633-644. Geological Society of London.

Hagevang, T., Eldholm, O., Aalstad, I., 1983. Pre-23 magnetic anomalies between Jan Mayen and Greenland-Senja Fracture Zones in the Norwegian Sea. Mar. Geophys. Res. 5, 345 – 363.

Hamann, N. E., Whittaker, R. C., Stemmerik, L., 2005. Geological development of the Northeast Greenland Shelf. In: Dore, A. G., Vining, B. A. (Eds.), Petroleum Geology: North-West Europe and Global Perspectives - Proceedings of the 6th Petroleum Geology Conference. Geol. Soc. Lond., 887 – 902.

Hansen, K., 1996. Thermotectonic evolution of a rifted continental margin: fission track evidence from the Kangerlussuaq area, SE Greenland. Terra Nova, 8(5), 458 – 469.

Hartley, R. A., Roberts, G. G., White, N., and Richardson, C., 2011. Transient convective uplift of an ancient buried landscape. Nature Geoscience, 4(8), 562-565.

Heiskanen, W. A. and F. A. Vening-Meinesz (1958). The Earth and its Gravity Field, 470 pp., McGraw-Hill, New York, Toronto and London.

Hermann, T., and Jokat, W., 2013. Crustal structures of the Boreas Basin and the Knipovich Ridge, North Atlantic. Geophysical Journal International, 193(3), 1399-1414.

Hinz, K., O. Endholm, M. Block, J. Skoseid, 1993. Evolution of North Atlantic volcanic continental margins. Petroleum Geology of Northwest Europe. In: Parker J. R. (ed.) Proceedings of the Fourth Conference. Geological Society, London, 901 – 913.

Hinz, K., Mutter, J.C., Zehnder, C.M. & Group, N.S., 1987. Symmetric conjugation of continent-ocean boundary structures along the Norwegian and East Greenland margins, Mar. Petrol. Geol., 3, 166 – 187.

Holford, S.P., Green, P. F., Duddy, I.R., Turner, J.P., Hillis, R.R., and Stoker, M.S., 2009. Regional intraplate exhumation episodes related to plate-boundary deformation. GSA Bulletin, 121(11/12), 1611 – 1628.

Husson, L., Yamato, P., and Bezos, A., 2015. Ultraslow, slow, or fast spreading ridges: Arm wrestling between mantle convection and far-field tectonics. Earth and Planetary Science Letters, 429, 205-215.

Hustoft, S., Mienert, J., Bünz, S., Nouzé, H., 2007. High-resolution 3D-seismic data indicate focussed fluid migration pathways above polygonal fault systems of the mid-Norwegian

margin. Marine Geology, Volume 245, Issues 1 – 4, 89-106, doi:10.1016/j.margeo.2007.07.004.

Iaffaldano, G. and Bunge, H.P., 2009. Relating rapid plate-motion variations to plate-boundary forces in global coupled models of the mantle/lithosphere system: Effects of topography and friction. Tectonophysics, 474(1-2): 393-404.

Iaffaldano, G., and H.-P. Bunge, 2015. Rapid Plate Motion Variations Through Geological Time: Observations Serving Geodynamic Interpretation. Annual Review of Earth and Planetary Sciences, 43:571–92.

Ito, G., 2001. Reykjanes' V'-shaped ridges originating from a pulsing and dehydrating mantle plume. Nature, 411(6838), 681-684.

Jakobsson, M., Backman, J., Rudels, B., Nycander, J., Frank, M., L.Mayer, Jokat, W., Sangiorgi, F., O'Reagan, M., Brinkhuis, H., King, J., Moran, K., 2007. The Early Miocene onset of a ventilated circulation regime in the Arctic Ocean. Nature 447, 986 – 990.

Japsen, P., Green, P.F., Bonow, J.M., Nielsen, T.F.D., Chalmers, J.A., 2014. From volcanic plains to glaciated peaks: Burial and exhumation history of southern East Greenland after opening of the NE Atlantic. Global Planet. Change 116, 91-114.

Japsen, P., Chalmers, J.A., Green, P.F., Bonow, J.M., 2012a. Elevated, passive continental margins: not rift shoulders, but expressions of episodic, post-rift burial and exhumation. Global Planet. Change, 90 – 91, 73 – 86.

Japsen, P., Green, P.F., Chalmers, J.A., 2012b. The mountains of North-East Greenland are not remnants of the Caledonian topography. A comment on Pedersen et al. (2012): Tectonophysics, 503 – 531, p. 318 – 330. Tectonophysics, 589, 234 – 238.

Japsen, P., Green, P.F., Nielsen, L.H., Rasmussen, E.S., and Bidstrup, T., 2007. Mesozoic-Cenozoic exhumation events in the eastern North Sea Basin: a multi-disciplinary study based on palaeothermal, palaeoburial, stratigraphic and seismic data. Basin Research, 2007, doi: 10.1111/j.1365-2117.2007.00329.x.

Japsen, P., Bonow, J.M., Green, P.F., Chalmers, J.A. & Lidmar-Bergström, K., 2006. Elevated, passive continental margins: Long-term highs or Neogene uplifts. New evidence from West Greenland. Earth Planet. Sc. Letters. 248, 315-324.

Johnson, C., Gallagher, K., 2000. A preliminary Mesozoic and Cenozoic denudation history of the North East Greenland onshore margin. Glob. Plan. Change, 24 (3 – 4), 261 – 274.

Jokat, W. et al., 2004. Reports on polar and marine research 475, Marine Geophysics, 475, 11 – 34.

Jokat, W. et al., 2003. Reports on polar and marine research. Marine Geophysics, 449, 8 – 27.

Jones, S. M., White, N., and Maclennan, J., 2002. V-shaped ridges around Iceland: Implications for spatial and temporal patterns of mantle convection. Geochemistry, Geophysics, Geosystems, 3(10), 1-23.

Jones, S. M., and White, N., 2003. Shape and size of the starting Iceland plume swell. Earth and Planetary Science Letters, 216(3), 271-282.

Jones, S.M., Murton, B.J., Fitton, J.G., White, N.J., Maclennan, J., and Walters, R.L., 2014. A joint geochemical – geophysical record of time-dependent mantle convection south of Iceland. Earth and Planetary Science Letters, 386, 86 – 97.

Knies, J., and Gaina, C., 2008. Middle Miocene ice sheet expansion in the Arctic: Views from the Barents Sea, Geochem. Geophys. Geosyst., 9, Q02015, doi:10.1029/2007GC001824.

Larsen, H.C., Saunders, A.D., 1998. Tectonism and volcanism at the SE Greenland rifted margin: a record of plume impact and later continental rupture. In: Wise, S. (Ed.), Proceedings of the Ocean Drilling Program, Scientific Results 152. Ocean Drilling Program, College Station, Texas, pp. 503 – 533.

Larsen, H.C., Saunders, A.D., Clift, P.D., Beget, J., Wei, W. and Spezzaferri, S., 1994. Seven million years of glaciation in Greenland. Science, 264, 5161, 952 – 955.

Larsen, R. B. and Tegner, C., 2006. Pressure conditions for the solidification of the Skaergaard intrusion: eruption of East Greenland flood basalts in less than 300,000 years. Lithos, 92(1), 181 – 197.

Libak, A., Eide, C.H., Mjelde, R., Keers, H., and Flüh, E.R. (2012). From pull-apart basins to ultraslow spreading: Results from the western Barents Sea Margin. Tectonophysics, 514 – 517, 44 – 61.

Lorenzo, J. M., Wessel, P., 1997. Flexure across a continent-ocean fracture zone: the northern Falkland/Malvinas Plateau, South Atlantic. Geo-Marine Letters 17, 110 – 118.

Lundin, E.R. and Doré, A.G., 2002. Mid-Cenozoic post-breakup deformation in the 'passive' margins bordering the Norwegian-Greenland Sea. Marine and Petroleum Geology, 19(1), 79 – 93.

Lundin, E.R. and Doré, A.G., 2011. Hyperextension, serpentinization, and weakening: A new paradigm for rifted margin compressional deformation. Geology, 39(4), 347 – 350.

Løseth, H., Henriksen, S., 2005. A Middle to Late Miocene compression phase along the Norwegian passive margin. In: Dore, A.G. & Vining, B.A. (Eds.), Petroleum Geology: North-West Europe and Global Perspectives - Proceedings of the 6th Petroleum Geology Conference. Geol. Soc. Lond., 845 – 859.

Mascle, J., Blarez, E., 1987. Evidence for transform margin evolution from Côte d'Ivorie-Ghana continental margin. Nature 326, 378 – 381.

Medhus, A.B., Balling, N., Jacobsen, B.H., Weidle, C., England, R.W., Kind, R., Thybo, H., Voss, P., 2012. Upper-mantle structure beneath the Southern Scandes Mountains and the Northern Tornquist Zone revealed by P-wave traveltime tomography. Geophys. J. Int. 189, 1315-1334.

Medvedev, S., Souche, A., and Hartz, E. H., 2013. Influence of ice sheet and glacial erosion on passive margins of Greenland. Geomorphology, 193, 36-46.

Merkouriev, S., DeMets, C., 2008. A high-resolution model for Eurasia–North America plate kinematics since 20 Ma. Geophys. J. Int. 173, 1064–1083.

Mjelde, R., and Faleide, J. I., 2009. Variation of Icelandic and Hawaiian magmatism: evidence for co-pulsation of mantle plumes?. Marine Geophysical Researches, 30(1), 61-72.

Molnar, P. and England, P. (1990). Late Cenozoic uplift of mountain ranges and global climate change: chicken or egg? Nature, 346, 6279, 29 – 34.

Mosar, J., Lewis, G., and Torsvik, T., 2002. North Atlantic seafloor spreading rates: implications for the Tertiary development of inversion structures of the Norwegian-Greenland Sea. J. Geol. Soc. Lond., 159, 503 – 515.

Myhre, A.M., Thiede, J., Firth, J.V., et al., 1995a. Site 913. In: Proceedings of the Ocean Drilling Program, Initial Reports, Vol. 151, 345 – 382. Ocean Drilling Program, College Station, TX.

Myhre, A.M., Thiede, J., Firth, J.V., et al., 1995b. Site 909. In: Proceedings of the Ocean Drilling Program, Initial Reports, Vol. 151, 159 – 220. Ocean Drilling Program, College Station, TX.

Nielsen, T., Knutz, P.C., and Kuijpers, A., 2008. Seismic expression of contourite depositional systems. Developments in Sedimentology, 60, 301 – 321.

Nielsen, S., Gallagher, K., Leighton, C., Balling, N., Svenningsen, L., Jacobsen, B., Thomsen, E., Nielsen, O., Heilmann-Clausen, C., Egholm, D., et al., 2009. The evolution of western Scandinavian topography: A review of Neogene uplift versus the ICE (isostasy-climate-erosion)-hypothesis. Journal of Geodynamics 47 (2 – 3), 72 – 95.

Olesen, O., Ebbing, J., Lundin, E., Mauring, E., Skilbrei, J. R., Torsvik, T. H., Hansen, E. K., Henningsen, T., Midboe, P. and Sand, M., 2007. An improved tectonic model for the Eocene opening of the Norwegian-Greenland Sea: Use of modern magnetic data. Marine and Petroleum Geology, 24, 53 – 66.

Parkin, C. J., and White, R. S., 2008. Influence of the Iceland mantle plume on oceanic crust generation in the North Atlantic. Geophysical Journal International, 173(1), 168-188.

Parnell-Turner, R., White, N., Henstock, T., Murton, B., Maclennan, J., and Jones, S. M., 2014. A continuous 55-million-year record of transient mantle plume activity beneath Iceland. Nature Geoscience.

Pedersen, V.K., Nielsen, S.B., and Gallagher, K., 2012. The post-orogenic evolution of the Northeast Greenland Caledonides constrained from apatite fission track analysis and inverse geodynamic modelling. Tectonophysics, 530, 318 – 330.

Poore, H. R., White, N., and Jones, S., 2009. A Neogene chronology of Iceland plume activity from V-shaped ridges. Earth and Planetary Science Letters, 283(1), 1-13.

Poore, H., White, N., and Maclennan, J., 2011. Ocean circulation and mantle melting controlled by radial flow of hot pulses in the Iceland plume. Nature Geoscience, 4(8), 558-561.

Poulsen, N.E., Manum, S.B., Williams, G.L., Ellegaard, M., 1996. Tertiary dinoflagellate biostratigraphy of Sites 907, 908, and 909 in the Norwegian-Greenland Sea. In: Thiede, J., Myhre, A.M., Firth, J.V., Johnson, G.L., Ruddiman, W.F. (Eds.), Proc. ODP, Sci. Results 151. Ocean Drilling Program, College Station, TX, pp.255–288.

Price, S., Brodie, J., Whitham, A. and Kent, R., 1997. Mid-Tertiary rifting and magmatism in the Traill Ø region, East Greenland. Journal of the Geological Society, London, 54, 419 – 434.

Ranero, C.R., Phipps Morgan, J., McIntosh, K., and Reichert, C., 2003. Bending-related faulting and mantle serpentinization at the Middle America trench. Nature, 425, 367 – 373.

Rasmussen, E.S., 2009. Neogene inversion of the Central Graben and Ringkøbing-Fyn High, Denmark. Tectonophysics 465, 84–97.

Reiners, P.W., Ehlers, T.A., Garver, J.I., Mitchell, S.G., Montgomery, D.R., Vance, J.A., Nicolescu, S., 2002. Late Miocene exhumation and uplift of the Washington Cascade Range. Geology 30, 767–770.

Rickers, F., Fichtner, A., Trampert, J., 2013. The Iceland – Jan Mayen plume system and its impact on mantle dynamics in the North Atlantic region: Evidence from full-waveform inversion, Earth and Planetary Science Letters, 367(1), 39 – 51.

Roberts, D.G., 1989. Basin inversion around the British Isles. In: Cooper, M.A. & Williams, D.G. (eds) Inversion Tectonics. Geological Society, London, Special Publications, 44, 131 – 150.

Rohrman, M. and van der Beek, P., 1996. Cenozoic postrift domal uplift of North Atlantic margins: An asthenospheric diapirism model. Geology, 24(10), 901 – 904.

Rudge, J. F., Champion, M. E. S., White, N., McKenzie, D., and Lovell, B., 2008. A plume model of transient diachronous uplift at the Earth's surface. Earth and Planetary Science Letters, 267(1), 146-160.

Rundberg, Y., and Eidvin, T., 2005. Controls on depositional history and architecture of the Oligocene-Miocene succession, northern North Sea Basin. Norwegian Petroleum Society Special Publications, 12, 207-239.

Sandwell, D., Schubert, G., 1982. Lithospheric flexure at fracture zones. J. Geophys. Res. 87 (B6), 4657 – 4667.

Shaw Champion, M. E., White, N. J., Jones, S. M., and Lovell, J. P. B., 2008. Quantifying transient mantle convective uplift: An example from the Faroe-Shetland basin. Tectonics, 27(1).

Srivastava, S.P. and Tapscott, C.R., 1986. Plate kinematics of the North Atlantic. In Vogt, P.R. and Tucholke, B.E. (eds) The Geology of North America, v. 1000, 379 – 404.

Steinberger, B., Spakman, W., Japsen, P. and Torsvik, T.H. (2015), The key role of global solid Earth processes in the late Cenozoic intensification of Greenland glaciation, Terra Nova, 27, 1-8, doi:10.1111/ter.12133

Stoker, M., Praeg, D., Shannon, P., Hjelstuen, B., Laberg, J., Nielsen, T., Van Weering, T., Sejrup, H., Evans, D., 2005. Neogene evolution of the Atlantic continental margin of NW Europe (Lofoten Islands to SW Ireland): anything but passive. In: Petroleum Geology: North West Europe and Global Perspectives: Proceedings of the 6th Conference. Geological Society of London, pp. 1057 – 1076.

Stoker, M. S., Holford, S. P., Hillis, R. R., Green, P. F., and Duddy, I. R., 2010. Cenozoic post-rift sedimentation off northwest Britain: Recording the detritus of episodic uplift on a passive continental margin. Geology, 38(7), 595-598.

Talwani, M. and O. Eldholm, 1977. Evolution of the Norwegian-Greenland Sea. Geological Society of America Bulletin, July, 1977, v. 88, p. 969-999, doi:10.1130/0016-7606(1977)88<969:EOTNS>2.0.CO;2

Thomson, K., Green, P. F., Whitham, A. G., Price, S. P., Underhill, J. R., 1999. New constraints on the thermal history of NE Greenland from apatite fission-track analysis. GSA Bulletin 111, 1054 – 1068.

Torsvik, T.H., Mosar, J., Eide, E.A., 2001. Cretaceous – Tertiary geodynamics: a North Atlantic exercise. Geophys. J. Int., 146, 850 – 866.

Torsvik, T. H., and Cocks, L. R. M., 2005. Norway in space and time: a centennial cavalcade. Norwegian Journal of Geology, 85(1-2), 73-86.

Vogt, P., 1986. Geophysical and geochemical signatures in plate tectonics. In: Hurdle, B. G. (Ed.), The Nordic Seas. Springer, New York, 413 – 662.

Voss, M., Schmidt-Aursch, M. & Jokat, W. 2009: Variations in magmatic processes along the East Greenland volcanic margin, Geophysical Journal International, 177, 755 – 782, doi:10.1111/j.1365-246X.2009.04077.x.

Vågnes, E., and Amundsen, H. E. F., 1993. Late Cenozoic uplift and volcanism on Spitsbergen: Caused by mantle convection?. Geology, 21(3), 251-254.

Walters, R. L., Jones, S. M., and Maclennan, J., 2013. Renewed melting at the abandoned Húnafloí Rift, northern Iceland, caused by plume pulsing. Earth and Planetary Science Letters, 377, 227-238.

Watts, A.B., 2001. Isostasy and flexure of the lithosphere. Cambridge University Press. 480 pages.

Weidle, C. and Maupin, V., 2008. An upper-mantle S-wave velocity model for Northern Europe from Love and Rayleigh group velocities. Geophys. J. Int, 175(3), 1154 – 1168.

Wessel, P. and Haxby, W.F., 1990. Thermal stresses, differential subsidence, and flexure at oceanic fracture zones. J. Geophys. Res., 95(B1), 375 – 391.

White, N., and Lovell, B., 1997. Measuring the pulse of a plume with the sedimentary record. Nature, 387(6636), 888-891.

Winkler, A., Wolf-Welling, T. C. W., Stattegger, K., Thiede, J., 2002. Clay mineral sedimentation in high northern latitude deep-sea basins since the Middle Miocene (ODP Leg 151, NAAG). Int. J. Earth Sci. 91(1), 133 – 148.

Wolfe, C.J., Bjarnason, I.T., VanDecar, J.C. and Solomon, S.C., 1997. Seismic structure of the Iceland mantle plume. Nature, 385, 245 – 247.

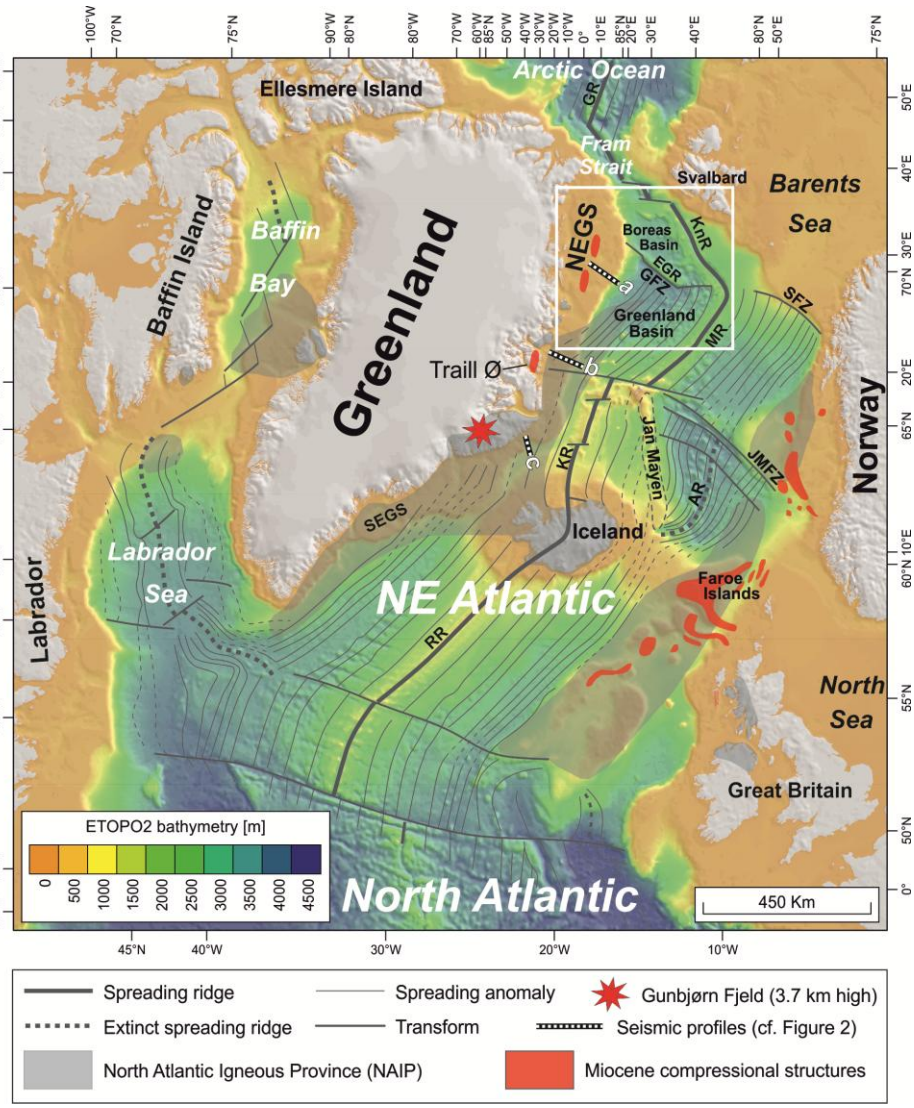

Figure 1. Tectonic and geological overview of the NE Atlantic – Labrador Sea/Baffin Bay area. Also shown are seafloor-spreading magnetic lineations (Lundin, 2002), extent of the North Atlantic Igneous Province (Nielsen et al., 2002) and (mainly early Miocene) compressional structures (Doré et al., 2008). Seismic profiles a, b, and c across the eastern shelves of Greenland is shown in Figure 2. White box: study area (see Figure 3). Abbreviations: AR, Aegir Ridge; EGR, East Greenland Ridge; GR, Gakkel Ridge; GFZ, Greenland Fracture Zone; JMFZ, Jan Mayen Fracture Zone; KnR, Knipovich Ridge; KR, Kolbeinsey Ridge; MR, Mohns Ridge; NEGS, North-East Greenland Shelf; RR, Reykjanes Ridge; SFZ, Senja Fracture Zone; SEGS, South-East Greenland Shelf.

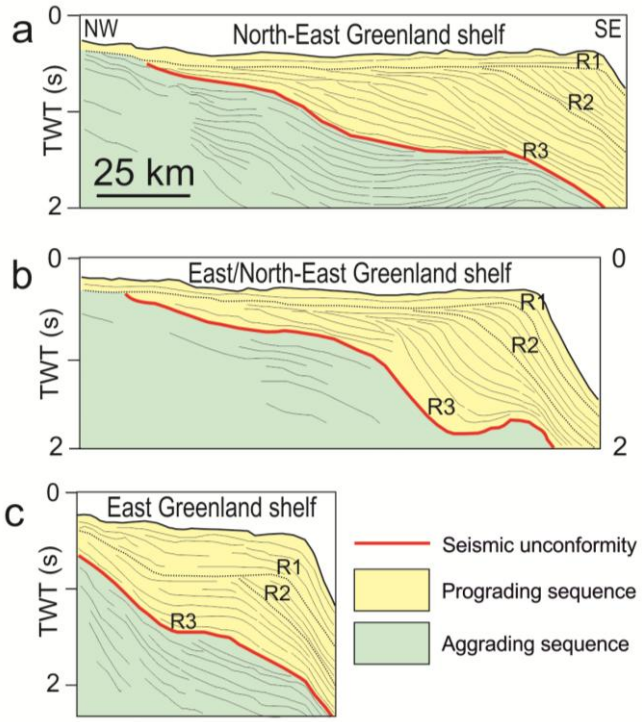

Figure 2. Line drawings of 2-D Multi-channel seismic (MCS) profiles a, b, and c from the eastern shelves of Greenland. Location of profiles in Figure 1. The profiles are redrawn from Berger and Jokat (2008; 2009) and are shown in same scale. Note the distinct, angular seismic unconformity that divides the Cenozoic sediments into an underlying, mainly aggrading sequence and an overlying, eastward prograding wedge. R1 – R3 denote subdivisions of the wedge by Berger and Jokat (2008; 2009).

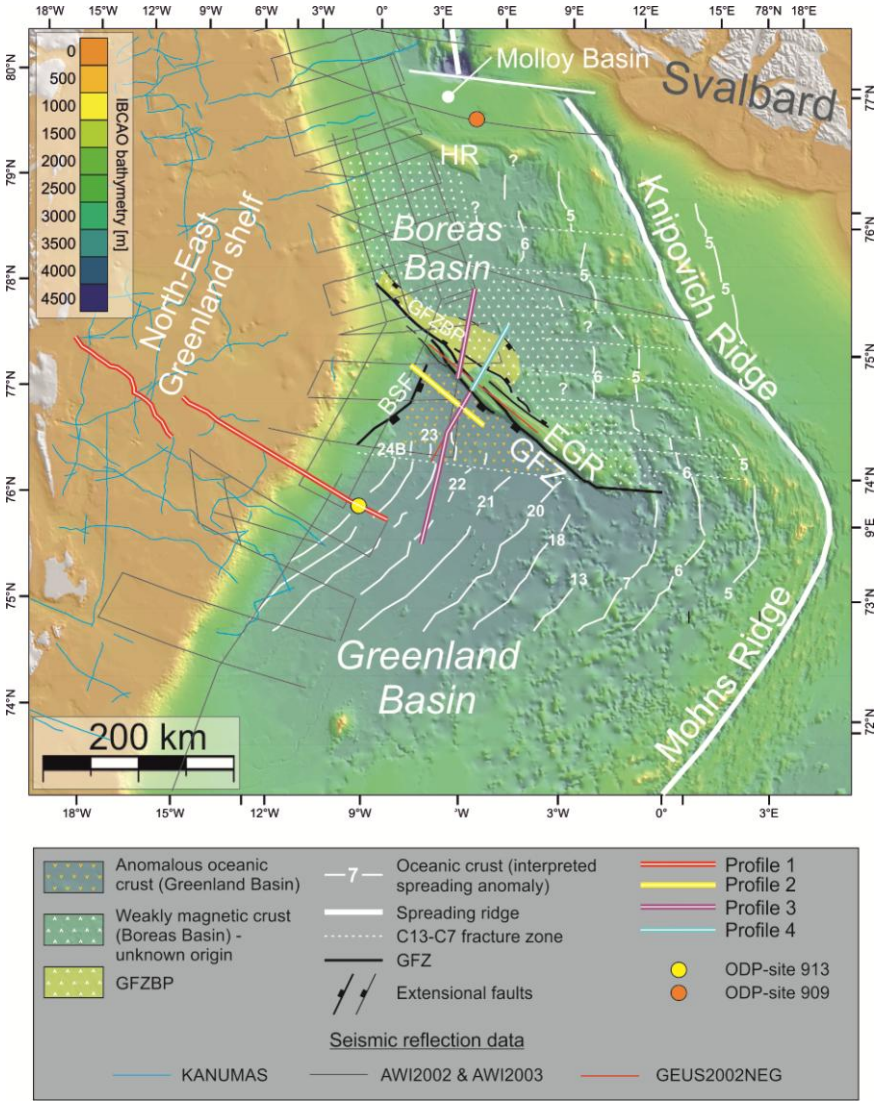

Figure 3. Map of study area showing structural-tectonic crustal features (location of area in Figure 1). Also shown is the available seismic reflection data. Bold lines highlight the seismic reflection Profiles 1 – 4 presented here. Background: IBCAO bathymetry (Jakobsson et al., 2012). Abbreviations: BSF, Base-of-slope fault; EGR, East Greenland Ridge; GFZ, Greenland Fracture Zone; GFZBP, Greenland Fracture Zone Basin Province. The structural-tectonic crustal interpretation is based on Døssing et al. (2008), Døssing and Funck (2012) and Gerlings et al. (2014) and modified according to interpretations presented by Døssing et al. (this study).

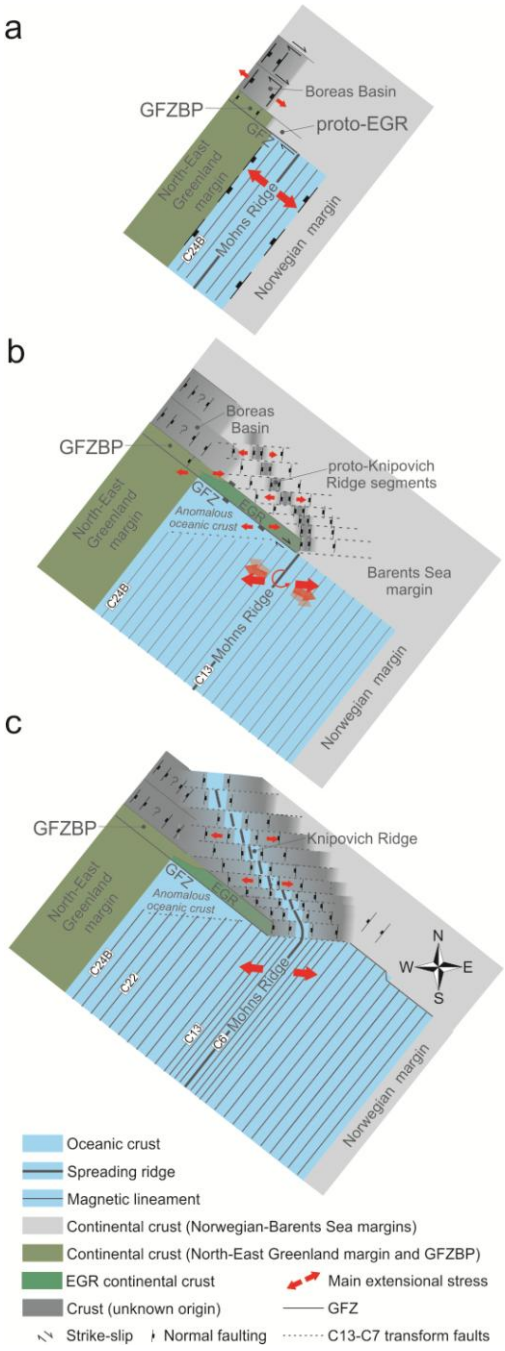

Figure 4. Simplified plate-kinematic model of the northern NE Atlantic. Modified after Mosar et al. (2002) and Døssing and Funck (2012) according to interpretations presented by Døssing et al. (this study). a, *Early to latest Eocene (chron C24B – C15; ~55 – 35 Ma)*: The GFZ acted as a left-lateral transfer zone between the Mohns Ridge and a zone of rifting – or spreading – in the western Boreas Basin. The GFZBP evolved as a deep, pull-apart basin along the northwestern segment of the GFZ. b, *Earliest to latest Oligocene (chron C13 – C7; ~35 – 24 Ma):* A counter-clockwise rotation of the lithospheric stress field promoted significant plate-motion changes and enforced extensional stresses across the GFZ-EGR

transform margin. The rift axis in the Boreas Basin jumped eastward to proto-Knipovich Ridge segments and eventually rifted of the continental EGR from the Barents Sea margin. East-west trending transform faults developed during this phase (e.g., Lundin and Doré, 2002; Døssing and Funck, 2012). c, *late early Miocene (chron C6; ~20 Ma)* or *late Miocene (chron C5; ~10.5 Ma)*: Merging of the Mohns and Knipovich spreading ridges and onset of present-day seafloor spreading. Abbreviations: EGR, East Greenland Ridge; GFZ, Greenland Fracture Zone; GFZBP, Greenland Fracture Zone Basin Province.

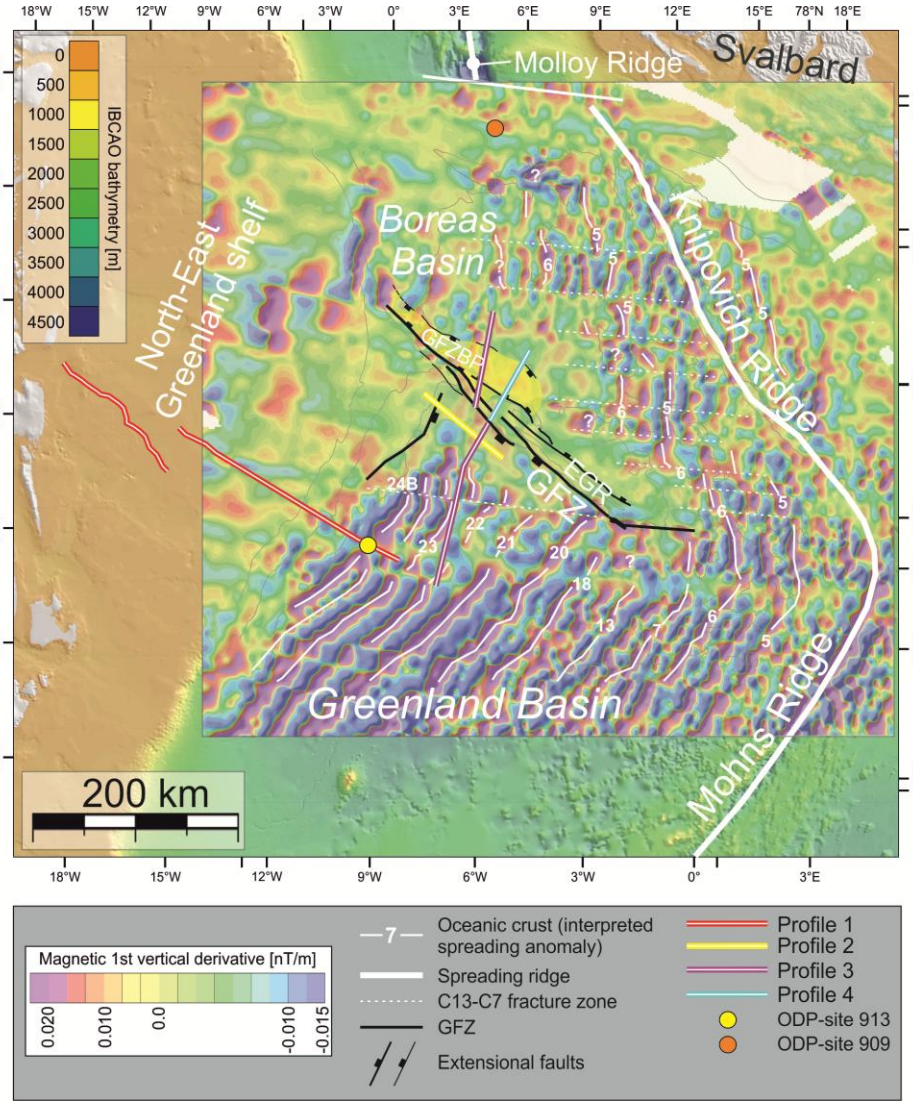

Figure 5. Map of 1st vertical derivative of magnetic anomalies (location of area in Figure 1). The magnetic data (Olesen et al., 2007) are superimposed on IBCAO bathymetry (Jakobsson et al., 2012). Magnetic isochrons interpretation modified after Vogt (1986) and Engen et al. (2008). Note that anomalies C6 and C5 define the first clear spreading anomalies on the Greenland side of the Knipovich Ridge. Magnetic anomalies older than anomaly C6 along Knipovich Ridge are weak, broken and highly ambiguous. Note also that well-defined seafloor spreading anomalies of the Greenland Basin terminate to the north against a triangular-shaped, weakly magnetic zone near the GFZ. The weakly magnetic crust correlates with elevated (5 – 8%) seismic P-wave velocities (Døssing et al., 2008).

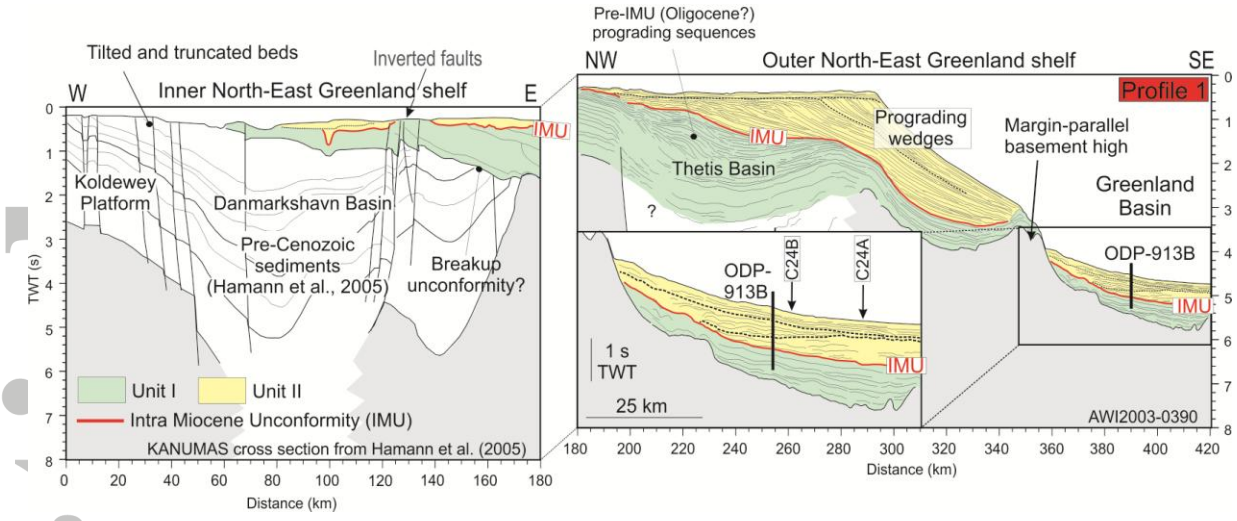

Figure 6. Profile 1 across the NE Greenland shelf (location in Figure 3). The inner shelf part of the profile is here presented as a seismic geo-section, originally compiled by Hamann et al. (2005) and based on confidential KANUMAS data. The remainder of the profile is composed by line AWI2003-0390 of the AWI2003 survey. The line-drawings in Profile 1 are redrawn from Hamann et al. (2005) and Berger and Jokat (2008), and the post-breakup stratigraphy beneath the NE Greenland shelf, as identified by mainly Hamann et al. (2005) and Berger and Jokat (2008; 2009), is used for our interpretation. Uninterpreted seismic data of line AWI2003-0390 is shown in Berger and Jokat (2008). Note the reverse faults that offset the IMU at km 125. Similar reverse faults have been mapped elsewhere on the shelf (Hamann et al., 2005). Correlation of the IMU from beneath the shelf and into the Greenland Basin is based on a seismic tie that circumvents the margin-parallel basement high at km 350 (Figures S1 and S2 in Supplementary Material). Inset: Zoom-in of the Greenland Basin-part of Profile 1. C23 and C24B: Identified magnetic spreading anomalies (Figure 5).

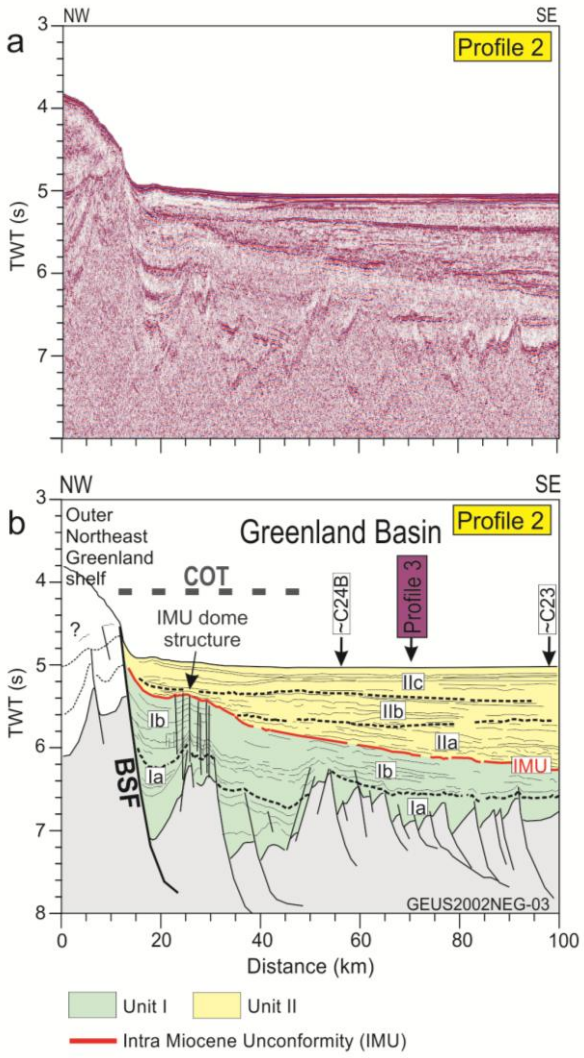

Figure 7. Profile 2 (location in Figure 3). a, Uninterpreted seismic profile. b, Line-drawing of seismic reflections. The IMU is traced from Profile 1 (Figure 6) via the AWI2003 survey (cf. Figure 3). Note the distinct tilt of the IMU and the underlying Subunits Ia and Ib. Note also the IMU compressional dome-structure at km 30. ~C23 and ~C24B refer to approximate location of magnetic spreading anomalies near this profile (cf. Figure 5). Abbreviations: BSF, Base-of-slope-fault; COT, Continent-Ocean Transition Zone.

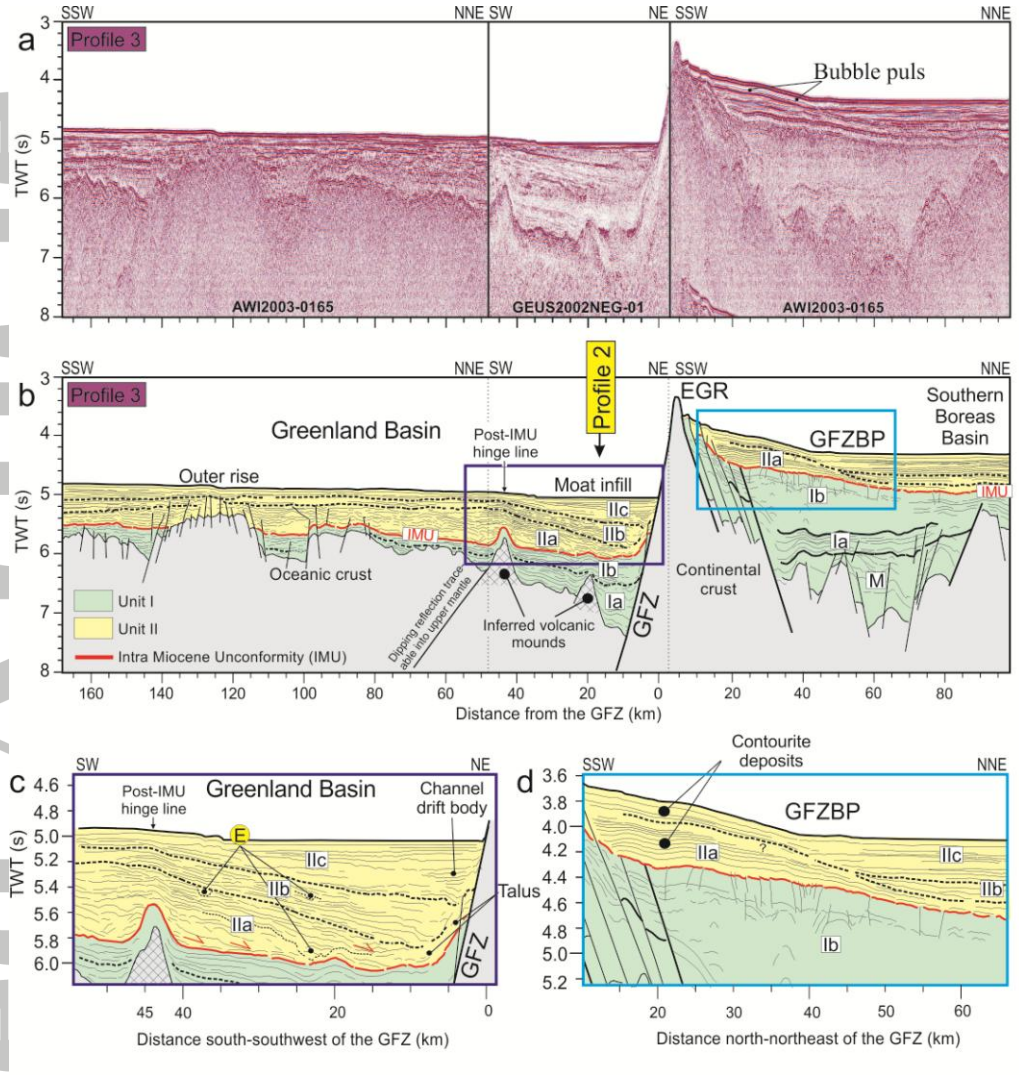

Figure 8. Profile 3 across the GFZ-EGR (location in Figure 3). a, Uninterpreted seismic profile. b, Line-drawings of seismic reflections. The IMU in the Greenland Basin has been traced from Profile 2 (Figure 7) and is tied to Profile 1 (Figure 6) and ODP-site 913 via the AWI2003 survey (cf. Figure 3; Berger and Jokat, 2008). The IMU in the GFZBP is tied to ODP-site 909 in the Molloy Basin via the AWI2002 survey (cf. Figure 3; Berger and Jokat, 2009). The deep, southwest-dipping intra-crustal reflection in the Greenland Basin near km 45 has been interpreted from Figure S2 in Supplementary Material. c, Zoom-in of moat infill against the GFZ-EGR. Note the apparent reflection downlap of Subunit IIa onto the IMU towards the GFZ and the buried channels (E) and their dipping flanks. d, Zoom-in of subunits above and below the IMU in the GFZBP. Note the flow structures in Subunit Ib, below the IMU, and the minor reverse faults that offset the IMU. Abbreviations: EGR, East Greenland Ridge; GFZ, Greenland Fracture Zone; GFZBP, Greenland Fracture Zone Basin Province.

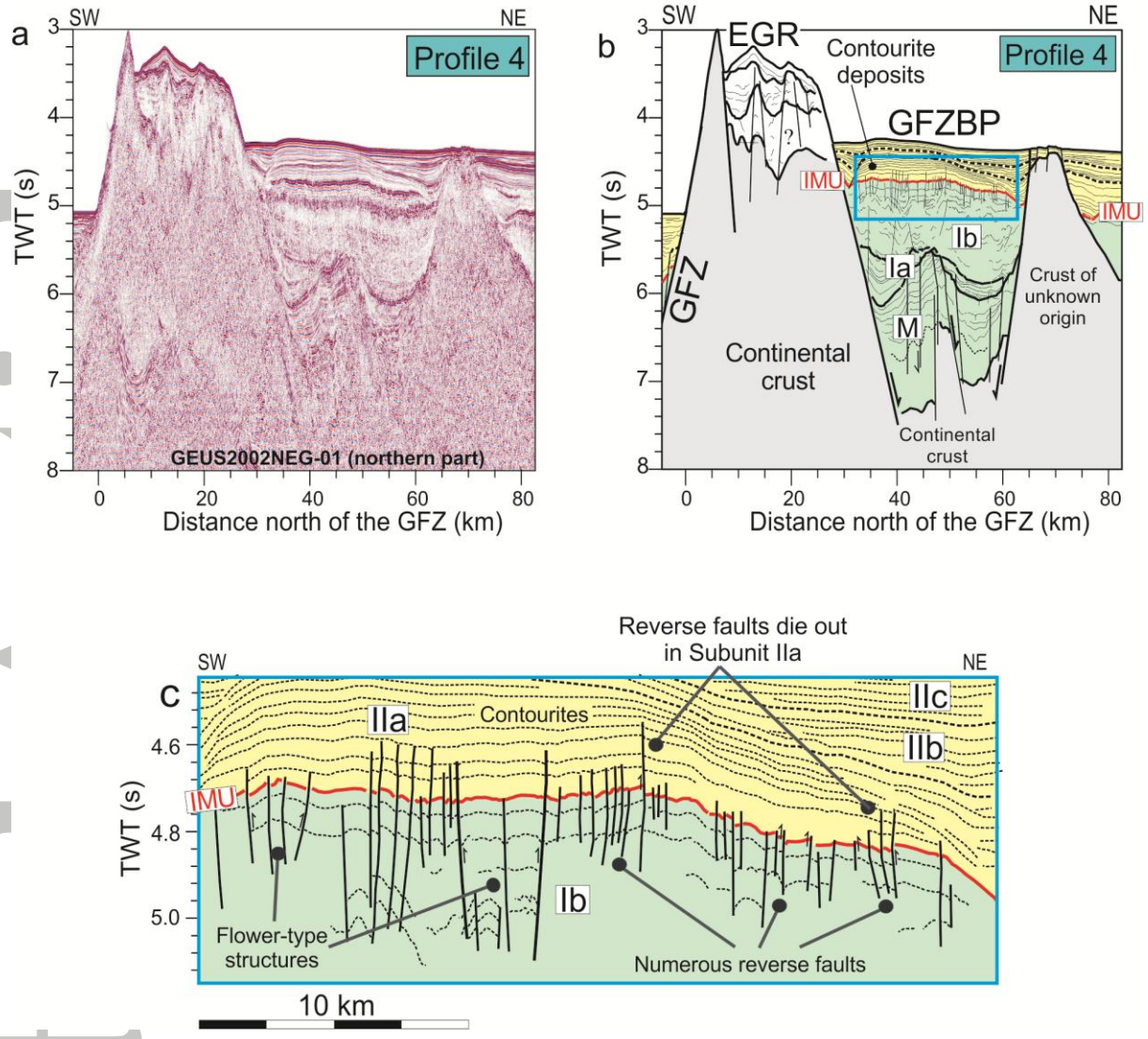

Figure 9. Profile 4 across the GFZ-EGR-GFZBP (location in Figure 3). a, Uninterpreted seismic profile. b, Line-drawings of seismic reflections. The IMU in the GFZBP is tied to ODP-site 909 via AWI2002 (Figure 3; Berger and Jokat, 2009). Note the overall convex-up, dome-shape structure of the IMU. Blue box: Zoom-in area of Figure 9c. c, Detailed interpretation of subunits below and above the IMU. Note the dense pattern of reverse faults that offset the IMU (vertical throw up to 50 m) and terminate in the contourite layer of Subunit IIa immediately above. Several, compressional flower-type structures are observed in Subunit Ib. Abbreviations: EGR, East Greenland Ridge; GFZ, Greenland Fracture Zone; GFZBP, Greenland Fracture Zone Basin Province.

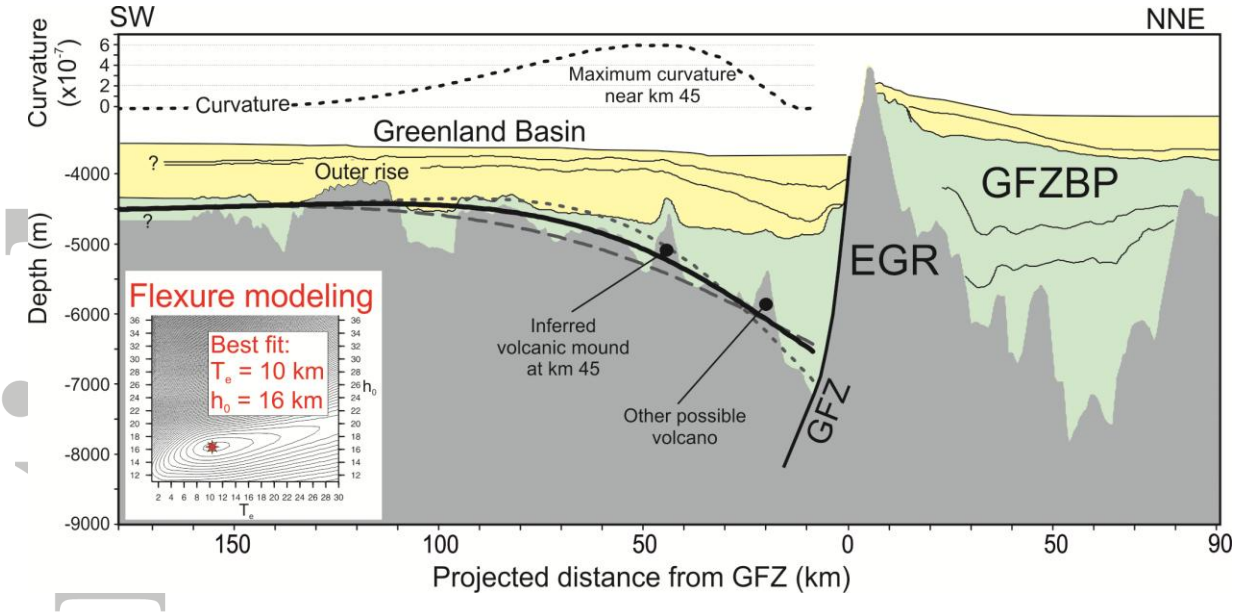

Figure 10. Results of 2-D flexure modeling along the Greenland Basin-part of Profile 3 (cf. Figure 8). Black bold line: Preferred fit of $T_{e(best)}$ = 10 km and $h_{0(best)}$ = 16 km, using a fault dip (θ) of 45° to the southwest. Gray dashed lines: Examples of alternative models with T_e = 14 km and T_e = 7 km. Inset: Plot misfit for various models of T_e versus h_0. Red star shows preferred model fit.

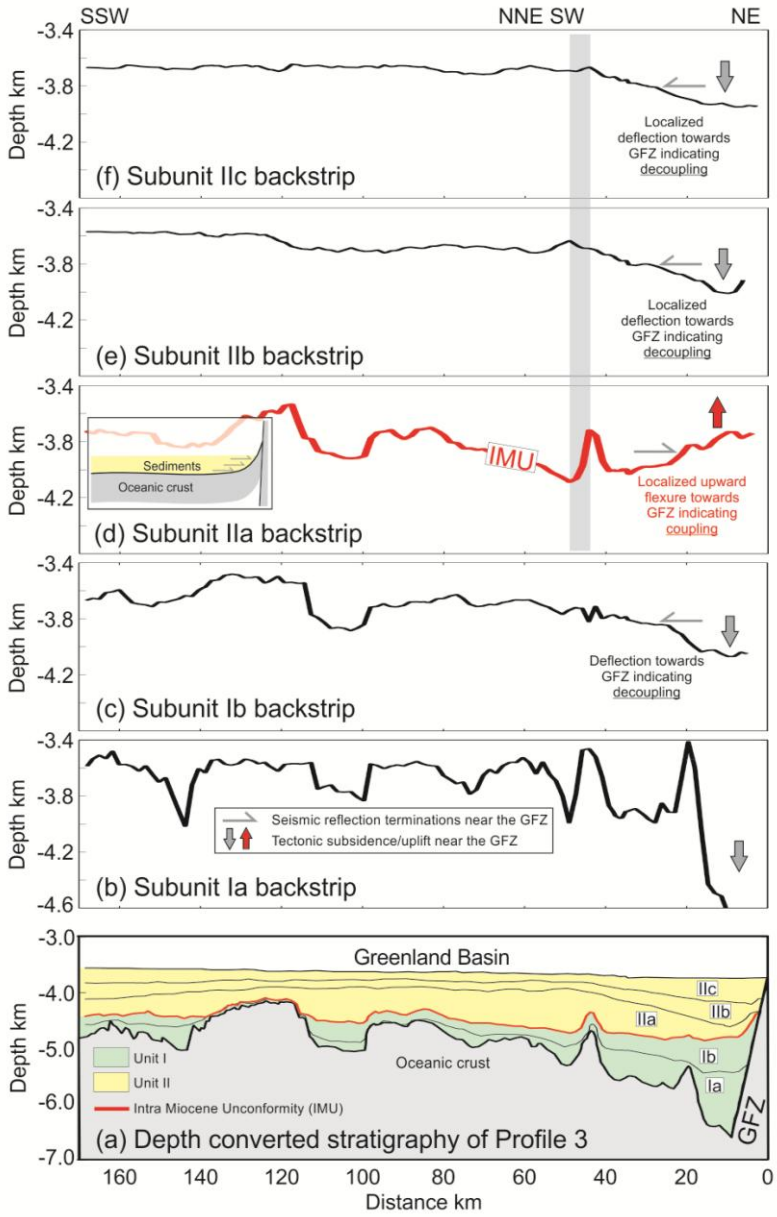

Figure 11. Results of 2-D flexural backstripping of sediment layers Greenland Basin-part of Profile 3 (cf. Figure 8). For the backstripping we have assumed an elastic thickness (T_e) of 10 km (Figure 10). Additional model parameter values are listed in Table 1. a, Depth converted stratigraphy with Subunits Ia, Ib, and IIa – IIc highlighted. b to f, Progressive backstrip results for Subunits Ia, Ib, IIa, IIb, and IIc. Also shown are the main seismic reflection terminations (gray arrows) for individual subunits near the GFZ. The reflection terminations are taken from Figure 8 and restored to the backstrip surfaces. In Figure 11d: Note the localized upward flexure of the IMU towards the GFZ and the restored onlap reflection terminations towards the GFZ. This pattern indicates thermo-mechanical coupling of the GFZ during continued differential thermal subsidence and deposition of Subunit IIa. Figure 11d – inset: Idealized setting of oceanic crust against a transform margin during thermo-mechanical

coupling and sediments that onlap progressively onto the localized upward-flexured underlying surface towards the transform. Vertical gray bar at km ~45 in Figures 11d to 11f denote location of a possible fault that cross-cutting the entire lithosphere and acted as a post-IMU weakness zone (Figure 8; Figure S4 in Supplementary Material). Plate note difference in vertical scales between Figure 11a and Figures 11b – 11f.

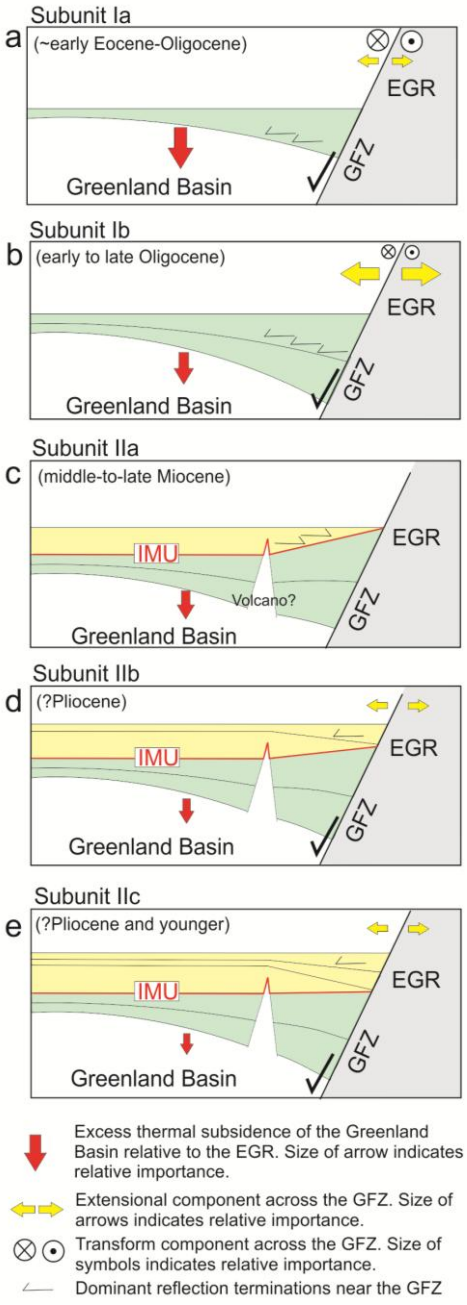

Figure 12. Summary sketch of tectonic subsidence history of the Greenland Basin against the GFZ-EGR. The figure is based on the seismic results of Døssing et al. (this study) and shows the evolution at five stages: (a) Subunit Ia (early Eocene to Oligocene), (b) Subunit Ib (early to late Oligocene), (c) Subunit IIa (midle-to-late Miocene), (d) Subunit IIb (?Pliocene), (e) Subunit IIc (?Pliocene and younger). Please note the IMU between Subunit Ib and Subunit IIa. The IMU defines the transition from thermo-mechanical decoupling to coupling across the GFZ. Note also the volcanic basement mound in (c) which reflects the basement feature observed 45 km to the south of the GFZ in Profile 3 (Figure 8). Abbreviations: EGR, East Greenland Ridge; GFZ, Greenland Fracture Zone, IMU, Intra Miocene Unconformity.

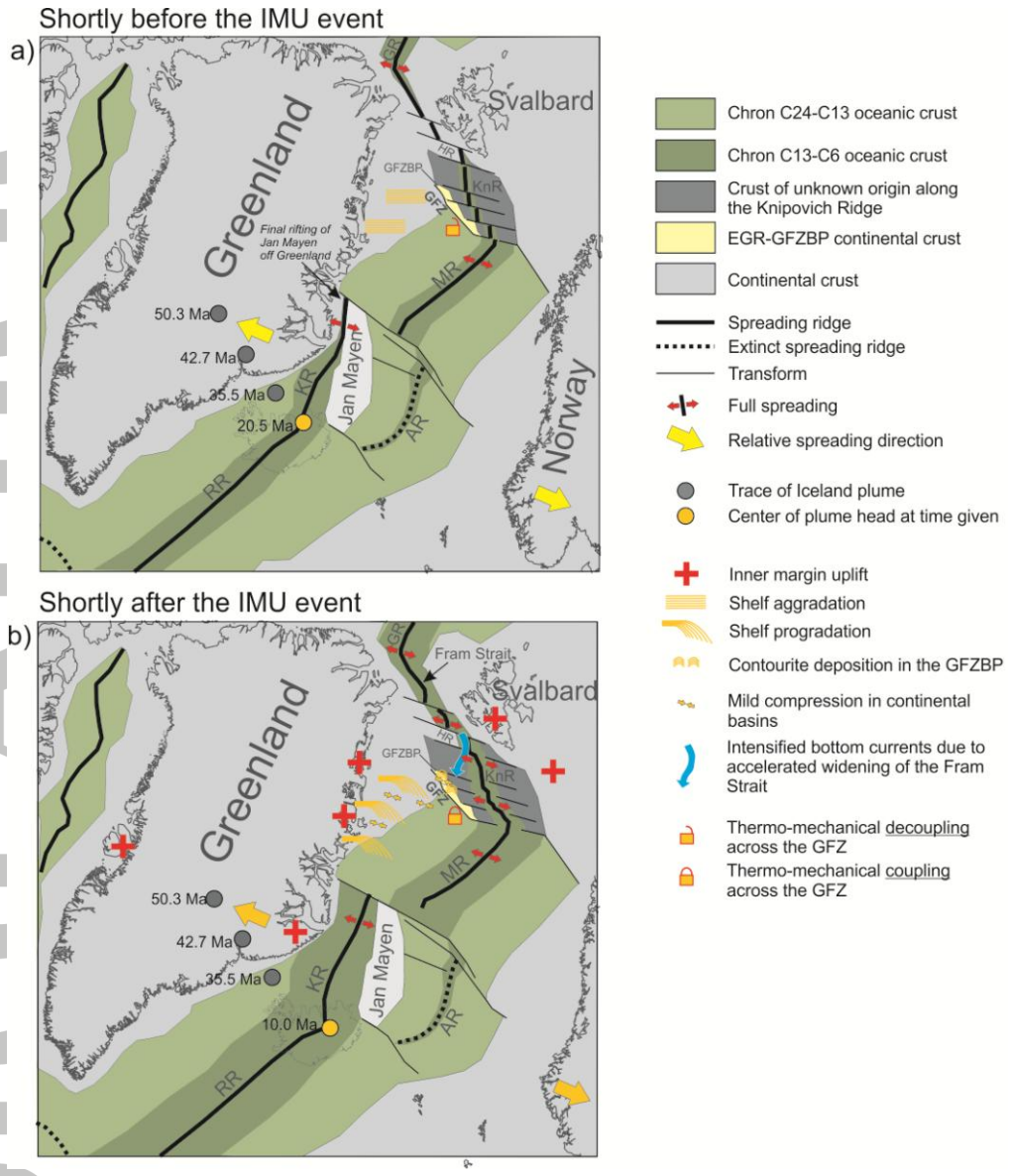

Figure 13. Simplified model showing interpreted plate tectonic and depositional settings of the NE Atlantic (a) shortly before and (b) shortly after the middle-to-late Miocene IMU event. The model is modified after Mosar et al. (2002) according to interpretations of Døssing et al. (this study). Note the change from thermo-mechanical decoupling to coupling across the GFZ and the associated onset of eastward shelf progradation in NE Greenland.
Abbreviations: AR, Aegir Ridge; EGR, East Greenland Ridge; GR, Gakkel Ridge; GFZ, Greenland Fracture Zone; GFZ, Greenland Fracture Zone Basin Province; KnR, Knipovich Ridge; KR, Kolbeinsey Ridge; MR, Mohns Ridge; RR, Reykjanes Ridge.

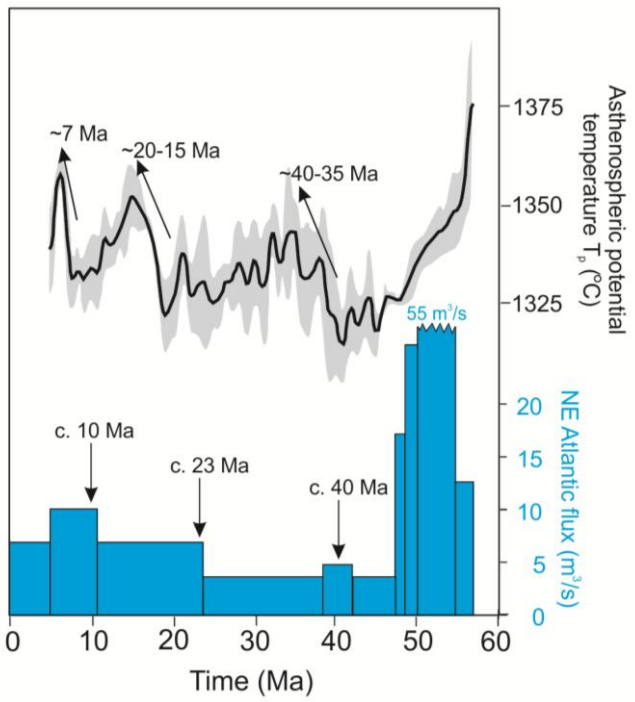

Figure 14. History of the Iceland plume fluctuations. Upper panel: Plume temperature fluctuations at the plume center (Parnell-Turner et al., 2015). Line with gray band, mean $\pm 1\sigma$ of T_p as function of time. Lower panel: Volume flux of the Iceland plume based on analyses of deep-seismic profiles across spreading ridges immediately to the north of Iceland (Mjelde and Faleide, 2009). Note the correlation between sharp changes in plume temperature and in volume flux at c. 23–15 Ma and c. 10–7 Ma. A less pronounced but still evident correlation is observed for the changes at c. 40–35 Ma.